AD_____

Award Number: W81XWH-09-1-0264

TITLE: Development of a novel NMR-based Rheb GTPase assay and molecular characterization of TSC2 GAP activity.

PRINCIPAL INVESTIGATOR: Vuk Stambolic, Ph.D.

CONTRACTING ORGANIZATION: University Health Network, Toronto
Toronto, Ontario M5G-2M9 Canada

REPORT DATE: May 2010

TYPE OF REPORT: Revised Final

PREPARED FOR: U.S. Army Medical Research and Materiel Command
Fort Detrick, Maryland 21702-5012

DISTRIBUTION STATEMENT: Approved for Public Release;
Distribution Unlimited

The views, opinions and/or findings contained in this report are those of the author(s) and should not be construed as an official Department of the Army position, policy or decision unless so designated by other documentation.

REPORT DOCUMENTATION PAGE

Form Approved
OMB No. 0704-0188

Public reporting burden for this collection of information is estimated to average 1 hour per response, including the time for reviewing instructions, searching existing data sources, gathering and maintaining the data needed, and completing and reviewing this collection of information. Send comments regarding this burden estimate or any other aspect of this collection of information, including suggestions for reducing this burden to Department of Defense, Washington Headquarters Services, Directorate for Information Operations and Reports (0704-0188), 1215 Jefferson Davis Highway, Suite 1204, Arlington, VA 22202-4302. Respondents should be aware that notwithstanding any other provision of law, no person shall be subject to any penalty for failing to comply with a collection of information if it does not display a currently valid OMB control number. **PLEASE DO NOT RETURN YOUR FORM TO THE ABOVE ADDRESS.**

1. REPORT DATE	2. REPORT TYPE	3. DATES COVERED
May 2010	Revised Final	1 May 2009 – 30 April 2010

4. TITLE AND SUBTITLE

Development of a novel NMR-based Rheb GTPase assay and molecular characterization of TSC2 GAP activity.

5a. CONTRACT NUMBER

5b. GRANT NUMBER
W81XWH-09-1-0264

5c. PROGRAM ELEMENT NUMBER

6. AUTHOR(S)

Vuk Stambolic, Ph.D.

E-Mail: grants@uhnresearch.ca

5d. PROJECT NUMBER

5e. TASK NUMBER

5f. WORK UNIT NUMBER

7. PERFORMING ORGANIZATION NAME(S) AND ADDRESS(ES)

University Health Network, Toronto
Toronto, Ontario M5G-2M9 Canada

8. PERFORMING ORGANIZATION REPORT NUMBER

9. SPONSORING / MONITORING AGENCY NAME(S) AND ADDRESS(ES)
U.S. Army Medical Research and Materiel Command
Fort Detrick, Maryland 21702-5012

10. SPONSOR/MONITOR'S ACRONYM(S)

11. SPONSOR/MONITOR'S REPORT NUMBER(S)

12. DISTRIBUTION / AVAILABILITY STATEMENT
Approved for Public Release; Distribution Unlimited

13. SUPPLEMENTARY NOTES

14. ABSTRACT

The biological activity of the tuberous sclerosis 1/2 complex (TSC1/TSC2), key molecules in the etiology of tuberous sclerosis, is sensitive to a number of homeostatic signals within the cell, including cellular energy levels, availability of oxygen and nutrients and growth factor stimulation. Mechanistically, TSC1 appears to protect TSC2 from proteolytic degradation, whereas TSC2 possesses GTPase activating protein (GAP) activity towards a small GTPase from the Ras superfamily named Rheb. We hypothesized that nuclear magnetic resonance (NMR) could be used to monitor Rheb's guanine nucleotide-dependent Rheb's structural changes, in real time, to provide a dynamic readout of its intrinsic and stimulated GTPase activity. Based on these principles we developed a real-time NMR-based GTPase assay which allows unprecedented insight into the molecular mechanism of action of GTPases and implemented it to characterize the molecular mechanism of GTP catalysis by Rheb and the impact of the TSC2 GAP activity on this process. Further, we characterized a series of TSC2 GAP domain mutants found in patients with tuberous sclerosis and determined the molecular mechanism of action of the TSC2 GAP activity on Rheb.

15. SUBJECT TERMS
TSC2, Rheb, NMR, catalytic activity, patient-associated mutations, GTPase

16. SECURITY CLASSIFICATION OF:			17. LIMITATION OF ABSTRACT	18. NUMBER OF PAGES	19a. NAME OF RESPONSIBLE PERSON
a. REPORT	b. ABSTRACT	c. THIS PAGE			USAMRMC
U	U	U	UU	31	19b. TELEPHONE NUMBER *(include area code)*

Table of Contents

Introduction

The biological activity of the tuberous sclerosis 1/2 complex (TSC1/TSC2), key molecules in the etiology of tuberous sclerosis, is sensitive to a number of homeostatic signals within the cell, including cellular energy levels, availability of oxygen and nutrients and growth factor stimulation. Mechanistically, TSC1 appears to protect TSC2 from proteolytic degradation, whereas TSC2 possesses GTPase activating protein (GAP) activity towards a small GTPase from the Ras superfamily named Rheb. We hypothesized that nuclear magnetic resonance (NMR) could be used to monitor Rheb's guanine nucleotide-dependent Rheb's structural changes, in real time, to provide a dynamic readout of its intrinsic and stimulated GTPase activity. We proposed to develop an assay based on this principle and use it to measure the GAP activity of TSC2 as well as its tuberous sclerosis-associated mutants.

Body

All of the tasks outlined in the approved Statement of Work have been accomplished, leading to one major publication (1) and two published follow-up studies (2, 3). A series of further studies, including the ones on the TC2-Rheb system and other GTPase and GAP/GEF pairs are being conducted and will likely lead to several future publications.

The details of the results of the proposed studies have been published (1) and can be found in the appendices. Progress on the specific tasks in briefly outlined bellow:

Task 1. Development of a dynamic, quantitative, time-resolved NMR-based GTPase assay for Rheb activity (months 1-4).

We expressed and purified Rheb 1-169 and collected of HSQC spectra of GDP- and GMPPNP-bound Rheb and determined its nucleotide-dependent structural changes. Based on these structures, we performed time-resolved collection of HSQC spectra of GTP-bound Rheb. Based on this data, we determined the intrinsic GTPase activity of Rheb.

Task 2. Characterization of the molecular determinants of GTP hydrolysis by Rheb and the mechanism of TSC2 GAP activity (months 5-8)

We expressed and purified various Rheb mutants and determined their GTPase activity using the NMR-based assay, exposing the molecular mechanism of GTP hydrolysis. Hydrolysis was also assessed in the presence of the TSC2 GAP domain, as well as a series of TSC2 GAP domain mutants found in patients with tuberous sclerosis. Assessment of the GAP-stimulated activity of Rheb, and that of several Rheb mutants designed to probe the mechanism of GAP/GTPase interaction allowed us to build a comprehensive structure-based model of the mechanism of nucleotide catalysis by Rheb.

Task 3. Biological characterization of TSC2 disease mutations affecting its GAP activity (months 9-12)

While the final aspects of this task are yet to be completed, we have successfully generated and confirmed expression of all the proposed TSC2 mutants and are in the final stags of characterizing the biological properties of the cells expressing them.

Key research accomplishments:

-development of a real-time NMR-based GTPase assay which allows unprecedented insight into the molecular mechanism of action of GTPases

-implementation of real-time NMR to characterize the molecular mechanism of GTP catalysis by Rheb and the impact of the TSC2 GAP activity on this process.

-characterization of a series of TSC2 GAP domain mutants found in patients with tuberous sclerosis.

-determination of the molecular mechanism of action of the TSC2 GAP activity on Rheb.

Reportable outcomes:

Publications:

1. Characterization of the intrinsic and TSC2-GAP-regulated GTPase activity of Rheb by real-time NMR. Marshall CB, Ho J, Buerger C, Plevin MJ, Li GY, Li Z, Ikura M, Stambolic V. Science Signaling. 2009 Jan 27;2(55):ra3.

2. Real-time NMR study of three small GTPases reveals that fluorescent 2'(3')-O-(N-methylanthraniloyl)-tagged nucleotides alter hydrolysis and exchange kinetics. Mazhab-Jafari MT, Marshall CB, Smith M, Gasmi-Seabrook GM, Stambolic V, Rottapel R, Neel BG, Ikura M. J Biol Chem. 2010 Feb 19;285(8):5132-6. Epub 2009 Dec 14.

3. Real-time NMR study of guanine nucleotide exchange and activation of RhoA by PDZ-RhoGEF. Gasmi-Seabrook GM, Marshall CB, Cheung M, Kim B, Wang F, Jang YJ, Mak TW, Stambolic V, Ikura M. J Biol Chem. 2010 Feb 19;285(8):5137-45. Epub 2009 Dec 17.

Funding:

A 3 year grant has been applied for and awarded to Dr. Mitsu ikura (Dr. Vuk Stambolic, co-applicant) from the Canadian Cancer Society Research Institute (formerly National Cancer Institute of Canada) for the implementation of real time NMR to the study of other GTPases, such as Rho and Ras. Results obtained in part through the DOD funding to Dr. Stambolic served as a proof of concept and were used as background information to justify the proposal. This funding mechanism does not ovelap with the DOD funding awarded to Dr. Stambolic.

Conclusion:

All the objectives of the proposed research were met and exceeded. The accomplished work provides an unprecedented mechanistic insight into the relationship between TSC2 and Rheb, a key node in the etiology of tuberous sclerosis.

References:

1. Characterization of the intrinsic and TSC2-GAP-regulated GTPase activity of Rheb by real-time NMR. Marshall CB, Ho J, Buerger C, Plevin MJ, Li GY, Li Z, Ikura M, Stambolic V. Science Signaling. 2009 Jan 27;2(55):ra3.

2. Real-time NMR study of three small GTPases reveals that fluorescent 2'(3')-O-(N-methylanthraniloyl)-tagged nucleotides alter hydrolysis and exchange kinetics. Mazhab-Jafari MT, Marshall CB, Smith M, Gasmi-Seabrook GM, Stambolic V, Rottapel R, Neel BG, Ikura M. J Biol Chem. 2010 Feb 19;285(8):5132-6. Epub 2009 Dec 14.

3. Real-time NMR study of guanine nucleotide exchange and activation of RhoA by PDZ-RhoGEF. Gasmi-Seabrook GM, Marshall CB, Cheung M, Kim B, Wang F, Jang YJ, Mak TW, Stambolic V, Ikura M. J Biol Chem. 2010 Feb 19;285(8):5137-45. Epub 2009 Dec 17.

Personnel who received salary support from the research effort:

Jason Ho
Dr Previn Dutt

GTP HYDROLYSIS

Characterization of the Intrinsic and TSC2-GAP–Regulated GTPase Activity of Rheb by Real-Time NMR

Christopher B. Marshall,[1,2] Jason Ho,[1] Claudia Buerger,[1,2] Michael J. Plevin,[1,2] Guang-Yao Li,[1,2] Zhihong Li,[1,2] Mitsuhiko Ikura,[1,2]* Vuk Stambolic[1,2]*

(Published 27 January 2009; Volume 2 Issue 55 ra3)

Tuberous sclerosis complex 2 (TSC2), whose gene is frequently mutated in tuberous sclerosis, increases the guanosine triphosphatase (GTPase) activity of the small heterotrimeric GTP-binding protein (G protein) Rheb, thus resulting in the decreased activity of the mammalian target of rapamycin (mTOR), the master regulator of cell growth. Here, we describe the development of a nuclear magnetic resonance (NMR)–based, quantitative, real-time assay to explore the molecular mechanism of the intrinsic and TSC2-catalyzed GTPase activity of Rheb. We confirmed that TSC2 accelerated GTP hydrolysis by Rheb 50-fold through an "asparagine-thumb" mechanism to substitute for the nonfunctional "catalytic" glutamine of Rheb and we determined that catalysis was enthalpy driven. Most, but not all, of the disease-associated GTPase-activating protein (GAP) domain mutants of TSC2 that we examined affected its enzymatic activity. This method can now be applied to study the function and regulation of other GTPases.

INTRODUCTION

Rheb is a conserved, ubiquitously expressed, small guanosine triphosphatase (GTPase) that belongs to the Ras superfamily and has homologs in yeast, fungi, slime mold, fruit fly, zebra fish, and mammals (*1*–*3*). Genetic and biochemical studies have firmly established Rheb as a molecular switch that acts immediately downstream of a protein complex consisting of the products of the tumor suppressor genes *tuberous sclerosis complex 1* (*TSC1*) and *TSC2* (*4*–*8*). Mutations in these genes are associated with tuberous sclerosis, a disorder characterized by benign tumors (hamartomas) that affect the brain, kidneys, skin, heart, and lungs (*9*, *10*). In the guanosine triphosphate (GTP)–bound state, Rheb assumes an "on" conformation and, through a largely unexplored molecular mechanism, potently activates the protein kinase mammalian target of rapamycin (mTOR), the master regulator of global cellular protein synthesis and growth (*11*). mTOR influences the extent of cellular protein translation by phosphorylation and inhibition of 4E-BP1, a negative regulator of eukaryotic translation initiation factor 4E (eIF4E) (*12*, *13*). Another mTOR target, p70S6 kinase (p70S6K), broadly influences translation through the phosphorylation and activation of eIF4B and inhibition of eIF2 kinase (*14*) (fig. S1).

TSC2 is a GTPase-activating protein (GAP) and mediates this effect by interacting with its target proteins through its C-terminal GAP domain, which is homologous to that of Rap1GAP (*7*–*10*). Upon interacting with TSC2, GTP hydrolysis by Rheb is accelerated, which results in a conformational transition to the guanosine diphosphate (GDP)–bound "off" state of Rheb (*15*) and decreased mTOR activity. TSC2 (also known as tuberin) heterodimerizes with TSC1 (also known as hamartin) (*16*) to form a complex that integrates a number of homeostatic signals within the cell, including growth factors, nutrients, oxygen, and cellular energy status (*11*, *17*–*21*) (fig. S1). In response to cytokines and growth factors, the stability of the complex is disrupted through the phosphorylation of TSC2 by Akt (*18*, *19*, *22*), extracellular signal–regulated kinase (ERK) (*23*), or ribosomal S6 kinase (RSK) (*24*), as well as through the phosphorylation of TSC1 by cyclin-dependent kinase 1 (CDK1) (*25*) or inhibitor of nuclear factor κB (IκB) kinase β (IKKβ) (*26*). On the other hand, the TSC1-TSC2 complex is stabilized when TSC2 is phosphorylated by adenosine monophosphate (AMP)–activated protein kinase (AMPK) or glycogen synthase kinase 3 (GSK-3) in response to depletion of cellular energy (*21*, *27*) or through its interaction with the protein regulated in development and DNA damage responses (REDD1) in response to hypoxia (*28*).

Rheb is most closely related to the small GTPases H-Ras and Rap2, but differences in some key amino acid residues suggest that Rheb has a unique molecular mechanism of action, in particular the presence of an arginine residue (Arg^{15}) in the conserved position homologous to Gly^{12} of Ras. Mutations in Gly^{12} of Ras hinder its intrinsic GTPase activity and decrease its susceptibility to the activity of RasGAP (*29*–*33*). Consistent with this, Rheb exhibits a lower intrinsic rate of GTPase activity than that of Ras; however, the substitution $Arg^{15}\rightarrow Gly^{15}$ is not sufficient to increase the GTPase activity of Rheb (*2*, *34*, *35*). Further, although Rheb has a potentially catalytic glutamine residue (Gln^{64}), which is equivalent to Gln^{61} of Ras, the crystal structure of Rheb shows that Gln^{64} is buried in a hydrophobic pocket in an orientation that is incompatible with any involvement in catalysis (*15*) (Fig. 1A).

The molecular parameters underlying the low intrinsic GTPase activity of Rheb are not well understood, and the mechanism by which TSC2 catalyzes GTP hydrolysis is not clear. To study these mechanisms, we took advantage of advances in nuclear magnetic resonance (NMR) spectroscopy to develop a quantitative, dynamic, structure-based, real-time enzymatic assay to measure the GTPase activity of Rheb. With this method, we obtained a time-resolved record of intrinsic hydrolysis of GTP by Rheb and determined the reaction rates of wild-type (WT) and mutant Rheb proteins, directly probing the molecular mechanism of hydrolysis. Moreover, we examined the GAP activity of several TSC2 polypeptides,

[1]Division of Signaling Biology, Ontario Cancer Institute, University Health Network, Toronto, Ontario, Canada M5G 2M9. [2]Department of Medical Biophysics, University of Toronto, Toronto, Ontario, Canada M5G 2M9.
*To whom correspondence should be addressed. E-mail: vuks@uhnres.utoronto.ca (V.S.) and mikura@uhnresearch.ca (M.I.)

Downloaded from stke.sciencemag.org on January 28, 2009

including disease-associated GAP domain mutants and engineered variants, providing a quantitative measure of their activity and dissecting the molecular mechanism of TSC2 GAP activity.

RESULTS

Structural distinction of nucleotide-dependent changes in Rheb by NMR

Based on the distinct structures of the crystalline forms of Rheb-GTP and Rheb-GDP (*15*), we anticipated that the NMR spectra of Rheb in solution would exhibit nucleotide-specific differences. We expressed the G-domain of Rheb (amino acid residues 1 to 169) in *Escherichia coli* and collected the ^{1}H-^{15}N heteronuclear single-quantum coherence (HSQC) NMR spectra of purified Rheb bound to either GDP or the nonhydrolyzable GTP analog guanosine 5′-[β,γ-imido]triphosphate (GMPPNP), respectively. The analysis of Rheb-GDP yielded a well-dispersed, high-quality HSQC spectrum (Fig. 1B), and backbone resonance assignments of about 140 peaks were obtained with standard triple-resonance NMR experiments (*36*) (fig. S2A). A stretch of residues within the switch II region (residues 66 to 73) could not be assigned because of peak broadening, which presumably arose from intermediate time-scale exchange between two or more conformational states. Analysis of Rheb-GMPPNP also produced a well-dispersed HSQC spectrum in which about half of the

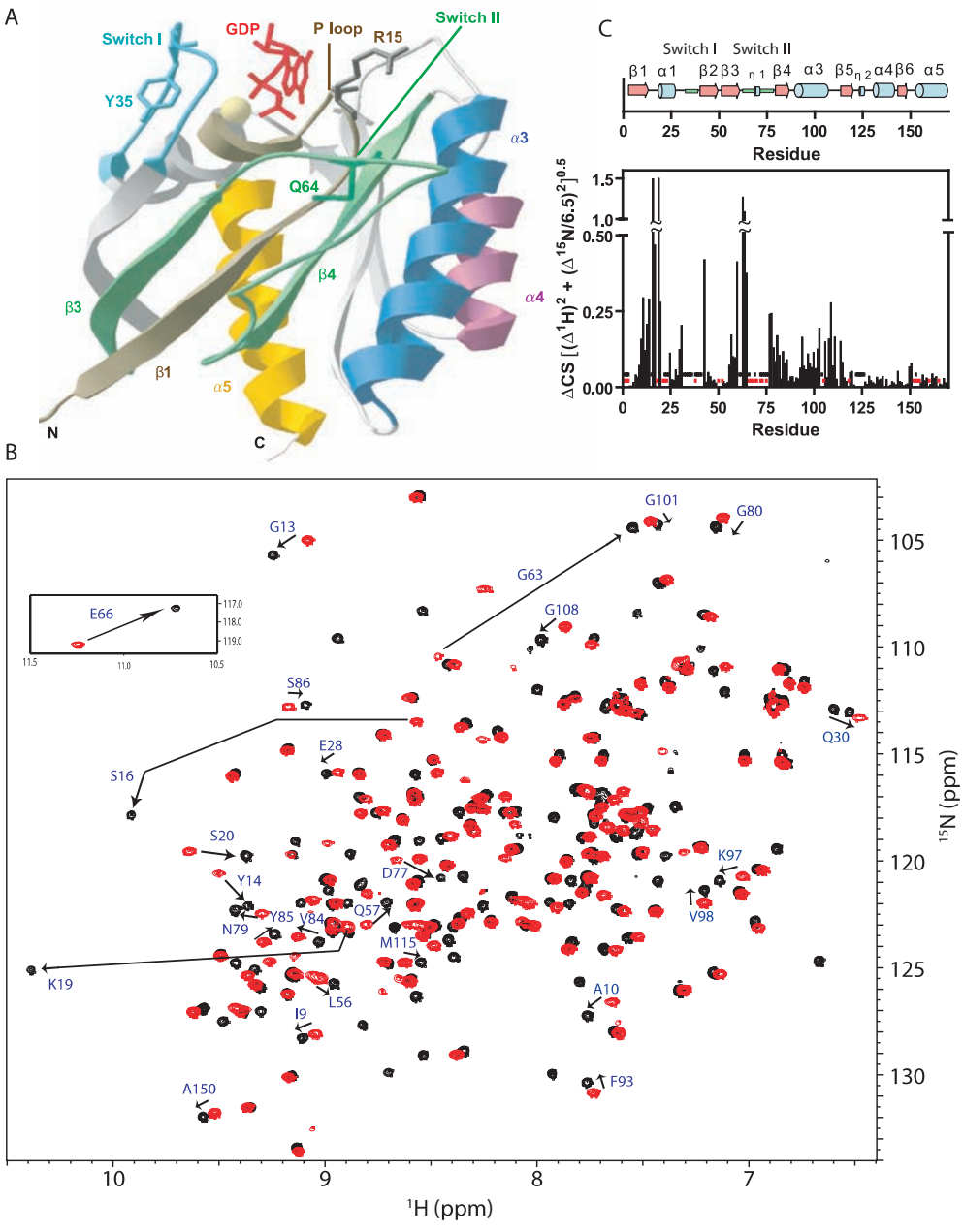

Fig. 1. Structure of Rheb and NMR spectral changes upon nucleotide cycling. (**A**) Crystal structure of Rheb-GDP [based on Protein Data Bank (PDB) 1XTQ (*15*)] with key structural elements and residues indicated. (**B**) ^{1}H-^{15}N HSQC spectra of Rheb in the GDP- and GMPPNP-bound states (black and red, respectively) with assignments of key residues and arrows to track changes in chemical shift. Full assignments are shown in fig. S2. Each spectrum represents an accumulation of 16 scans requiring a collection time of 80 min. (**C**) Secondary structure of Rheb and changes in chemical shift for Rheb-GDP versus Rheb-GMPPNP. Where residues were assigned in both spectra, normalized changes in chemical shift were calculated. Blue dots indicate residues that were not assigned in the GMPPNP-bound state and red dots indicate those residues that were not assigned for Rheb-GDP.

Downloaded from stke.sciencemag.org on January 28, 2009

peaks exhibited chemical shift changes relative to those of Rheb-GDP, whereas a number of peaks were nearly superimposable on those of the Rheb-GDP spectrum (Fig. 1B). Broadening or complete loss of peaks were also observed. Residue-specific assignment was possible for 130 cross peaks in the ^{1}H-^{15}N HSQC spectrum of GMPPNP-bound Rheb (fig. S2B); however, residues corresponding to the switch I region (residues 31 to 42) were broadened and could not be assigned. This observation is consistent with the conformational heterogeneity of the switch regions seen in other GTPases (*37*).

Comparison of the HSQC spectra of GDP- and GMPPNP-bound Rheb identified elements associated with nucleotide-dependent structural changes. Specifically, amino acid residues in and around the nucleotide-binding pocket, including the P loop (residues 10 to 20) and switch II region (residues 60 to 65) displayed prominent changes in chemical shift (Fig. 1C). Chemical shift index (CSI) values (*38*) calculated for the assigned residues were in full agreement with the secondary structures of Rheb previously determined by x-ray crystallography (*15*) (fig. S3).

Development of a real-time, NMR-based assay for the analysis of the GTPase activity of Rheb

Because our HSQC spectra distinguish Rheb bound to the GTP analog from GDP-bound Rheb, we set out to monitor the change in the relative proportions of GTP-bound and GDP-bound Rheb over time as a way to measure the GTPase activity of Rheb. To load Rheb with unmodified GTP, it was incubated overnight with a 10-fold excess of GTP in the presence of 10 mM EDTA to promote nucleotide exchange and then saturated with Mg^{2+} and desalted by gel filtration (*39*) (fig. S4). EDTA was used to chelate Mg^{2+} and weaken the binding of nucleotide, whereas the subsequent addition of Mg^{2+} served to stabilize GTP binding to Rheb. The resulting Rheb preparations were typically >90% loaded with GTP (determined from peak ratios in ^{15}N HSQC spectra) and produced HSQC spectra similar to those of Rheb-GMPPNP.

To probe the intrinsic GTPase activity of Rheb in real time, multiple ^{15}N HSQC spectra of freshly prepared Rheb-GTP (400 μM, at 19°C) were collected successively during the hydrolysis reaction, initially every 5 min and then with decreasing frequency. The combination of high-field NMR (800 MHz) and a highly sensitive cryoprobe allowed us to collect reproducible spectra with high signal-to-noise ratios in less than 5 min (Fig. 2A). The first spectrum consisted of prominent cross peaks corresponding to Rheb-GTP with a subset of cross peaks from Rheb-GDP visible just above the noise level. As the hydrolysis of nucleotide proceeded, peaks corresponding to Rheb-GDP increased in intensity, while the peaks corresponding to Rheb-GTP decreased. Both sets of peaks exhibited similar intensities at ~12 hours, and by 44 hours the peaks corresponding to Rheb-GTP were reduced to the level of noise, indicating the complete turnover of GTP (Fig. 2A and fig. S5).

The intensities of each Rheb-GTP and Rheb-GDP cross peak were extracted from the spectra collected at each time point and the peak heights of well-resolved "reporter residues" were plotted against time (fig. S6). Peak heights corresponding to Rheb-GTP or Rheb-GDP were normalized to the initial spectrum (GTP-bound) and the final spectrum (GDP-bound), respectively, and well-resolved peaks were grouped based on their position within the structure of Rheb. Amino acid residues in each of four regions, (i) the β1 strand and the P loop, (ii) the switch I region, (iii) the β3 strand, the switch II region, and the β4 strand, and (iv) the α3 helix produced GTP-specific peaks that decreased in intensity with single-phase exponential decay kinetics and GDP-specific peaks that appeared with the same kinetics (Fig. 2B). These structural elements were near the nucleotide-binding site or the switch regions, consistent with the notion that the observed changes in NMR spectra reflect the GTPase reaction.

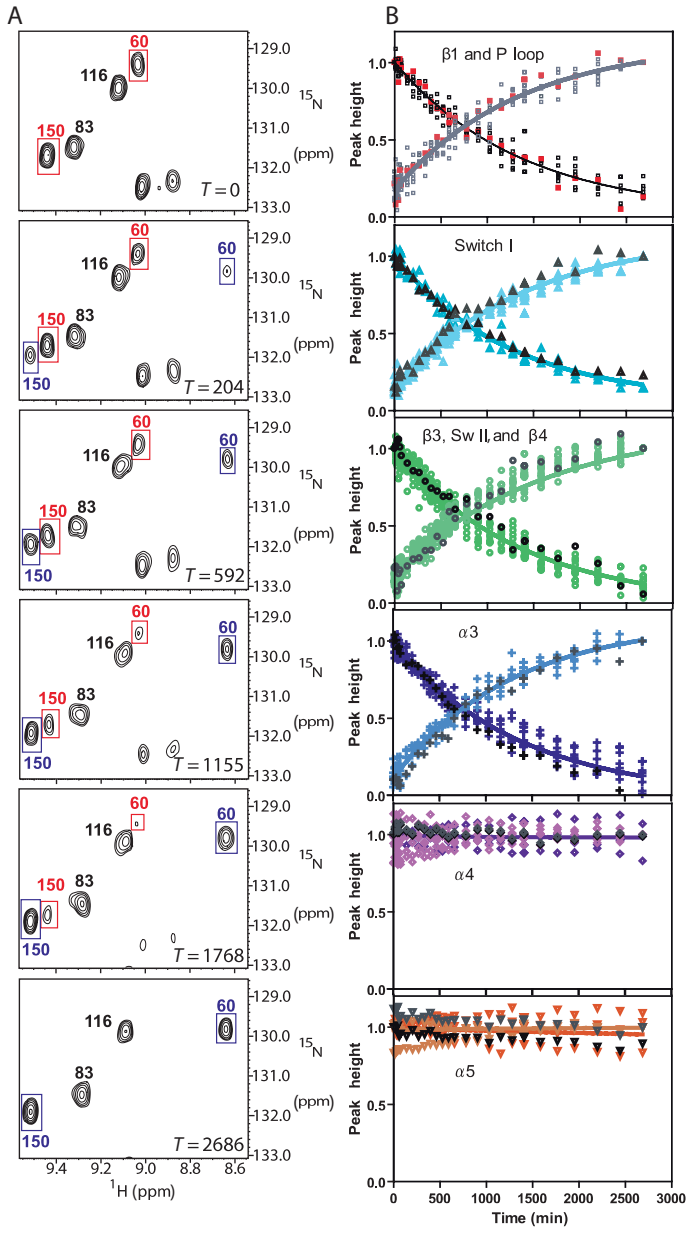

Fig. 2. Intrinsic GTPase activity of Rheb. (**A**) Snapshots of the HSQC spectra of GTP-loaded Rheb taken throughout the time course of GTP hydrolysis (time indicated in minutes). Peaks specific to Rheb-GTP are indicated in red, peaks corresponding to Rheb-GDP that appear as hydrolysis occurs are indicated in blue, and peaks that do not change with hydrolysis are labeled in black. (**B**) Peak heights for Rheb residues corresponding to GTP-bound (dark colors, normalized to T = 0) and GDP-bound (light colors, normalized to the end point of the hydrolysis reaction) states versus time. Residues are grouped according to structural elements and are colored to correspond to Fig. 1A. For each region, data points for a single residue are indicated in red or black (Y14, F31, Q57, K97, Q139, and A167). These data are derived from a representative GTPase experiment, with each time point representing two scans collected over 5 min.

Downloaded from stke.sciencemag.org on January 28, 2009

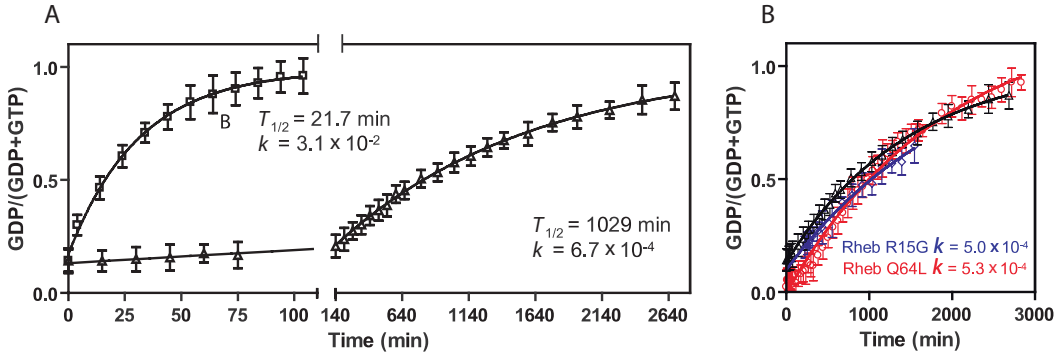

Fig. 3. Intrinsic GTPase activity and sensitivity to GAP activity of WT and mutant Rheb. (A) Hydrolysis of GTP by WT Rheb alone (triangles) or in the presence of $TSC2_{1525–1742}$ (squares) presented as a fraction of GDP for each time point based on peak heights $[I_{GDP}/(I_{GDP} + I_{GTP})]$ averaged for 22 residues. Error bars represent standard deviation of the fraction of GDP reported by the 22 residues. (B) Intrinsic GTPase activity of Rheb mutants R15G (blue diamonds) and Q64L (red circles) compared to that of WT Rheb (black triangles). Each curve is derived from a representative GTPase assay with multiple time points, each representing two scans.

In contrast, peaks corresponding to residues in the α4 and α5 helices displayed nearly identical positions and intensities (Fig. 2B). In total, dynamic changes in 22 amino acid residues of Rheb were used to derive a single curve reflective of the GTPase reaction (Fig. 3A). The fraction of Rheb bound to GDP was calculated on the basis of the intensity of each of the 22 peaks $[I_{GDP}/(I_{GDP} + I_{GTP})]$ at each time point and the averaged data fit an exponential decay curve with a rate of 6.7×10^{-4} min^{-1}, indicative of a GTP half-life of 1029 min (Fig. 3A).

Atypical of Ras subfamily members, Rheb contains an arginine residue (Arg^{15}) (Fig. 1A) at a position in which glycine is conserved (for example, Gly^{12} in Ras). Mutations of Gly^{12} (including Gly^{12}→Arg^{12}) reduce the intrinsic GTPase activity of Ras and severely impair the ability of RasGAPs to promote GTP hydrolysis by Ras (*30–33*, *40–43*). In mammalian cells, Rheb proteins with mutations in Arg^{15} exhibit similar GTP loading to WT Rheb and no difference in downstream signaling processes; however, the Rheb Arg^{15}→Gly^{15} mutant is partially resistant to the GAP activity of overexpressed TSC2 (*34*, *35*). To examine the importance of Arg^{15} for GTP hydrolysis, the GTPase activity of the Arg^{15}→Gly^{15} mutant Rheb was assessed by NMR. Consistent with previous studies, we found that this "Ras-like" mutation did not improve the catalytic activity of Rheb. Rather, this mutation decreased the intrinsic GTPase activity of Rheb by 25% (Fig. 3B), which has not been previously reported likely due to the limitations of thin-layer chromatography (TLC) as a detection method for measuring GTPase activity. Relative to the effect of mutation of the catalytic Gln^{61} of Ras, mutation of the homologous residue (Gln^{64}) in Rheb has less effect on GTP loading (*35*); however, the cell-based assay used could not completely distinguish between the effects of the mutation on the intrinsic GTPase activity of Rheb and those that affected the sensitivity of Rheb to GAP activity. Based on its orientation in the solved crystal structure of Rheb, it has been suggested that Gln^{64} may not participate in the hydrolysis of GTP (*15*). In our assay, a Gln^{64}→Leu^{64} mutant of Rheb had only slightly decreased catalytic activity compared to that of WT Rheb (Fig. 3B), further supporting the conclusion that, unlike in Ras, the conserved glutamine is not involved in hydrolysis. Taken together, these data provide a dynamic and quantitative measure of the GTPase activity of Rheb that is in full agreement with previous in vivo and in vitro studies, thus suggesting that our assay would also be useful for the study of the GAP activity of TSC2.

Characterization of the TSC2-GAP–catalyzed GTPase activity of Rheb

To investigate the activity and mechanism of action of the GAP domain of TSC2 (TSC2-GAP) with our NMR-based assay, various TSC2-GAP domain polypeptides were designed in light of its predicted secondary structure and homology to Rap1GAP. Among the constructs tested, we found that a polypeptide consisting of amino acid residues 1525 to 1742 of TSC2 ($TSC2_{1525–1742}$) exhibited the best expression and stability in *E. coli*. The N-terminal boundary of this construct was chosen so as to encompass all residues homologous to the catalytic domain of Rap1GAP. The C terminus of the construct was limited by the presence of a proteolytically labile site, which we identified by mass spectrometry as the Ala^{1742} to Arg^{1743} peptide linkage. Addition of $TSC2_{1525–1742}$ to Rheb-GTP at a 1:2 molar ratio increased Rheb's rate of GTP hydrolysis by 50-fold to 3.1×10^{-2} min^{-1} (Fig. 3A). Apart from accelerating the conversion of Rheb-GTP to Rheb-GDP, the GAP domain of $TSC2_{1525–1742}$ did not cause any discernable changes in the HSQC spectrum. Even when the GAP domain of $TSC2_{1525–1742}$ was added to GMPPNP-bound Rheb at a 1:1 molar ratio, no changes in the HSQC spectrum of Rheb were detected.

To assess the thermodynamic properties of the intrinsic and GAP-accelerated GTPase activities of Rheb, we examined the hydrolysis of GTP by Rheb alone and in the presence of the GAP domain of $TSC2_{1525–1742}$ at different temperatures. Using Arrhenius plots of reaction rate versus temperature (Fig. 4A), we calculated thermodynamic activation parameters for the hydrolysis of GTP, which allowed us to probe the unstable transition state that represents an energy barrier on the reaction pathway toward product formation. The minimum energy required to drive the reaction beyond this threshold is called the activation enthalpy ($\Delta H^{\ddagger}$). The reaction rate also depends on the activation entropy ($\Delta S^{\ddagger}$): the difference in entropy between the ground state and the transition state. Large negative values of $\Delta S^{\ddagger}$ indicate that disorder is reduced upon formation of the transition state, which is unfavorable for catalysis. Enzymes generally decrease $\Delta G^{\ddagger}$, the free energy of activation ($\Delta G^{\ddagger} = \Delta H^{\ddagger} - T\Delta S^{\ddagger}$), through stabilization of the transition state, which lowers the enthalpic component ($\Delta H^{\ddagger}$). Compared to the hydrolysis of GTP in water, Rheb reduces $\Delta H^{\ddagger}$ by 16.9 kJ/mol with little effect on $\Delta S^{\ddagger}$, thus reducing $\Delta G^{\ddagger}$ by 16.7 kJ/mol (Fig. 4B). Ras also promotes hydrolysis of GTP by reducing $\Delta H^{\ddagger}$, but to a greater extent than does Rheb (−21.5 kJ/mol) (*44*), resulting in a markedly faster reaction rate. The addition of substoichiometric quantities of the GAP domain of $TSC2_{1525–1742}$ (1:7 molar ratio) to Rheb further lowered $\Delta G^{\ddagger}$ by 6.8 kJ/mol at 25°C, consistent with the 50-fold increase in reaction rate. A substantial reduction in activation enthalpy by TSC2-GAP ($\Delta\Delta H^{\ddagger} = -46.3$ kJ/mol) was largely offset by an unfavorable decrease in activation entropy ($-T\Delta\Delta S^{\ddagger} = 39.5$ kJ/mol at 25°C), resulting in the modest overall reduction in free energy of activation. Taken together, the observed decreases in the enthalpic barriers for GTP hydrolysis by Rheb and Rheb–TSC2-GAP complex are consistent with a conventional enzymatic mechanism involving stabilization of the transition state.

Downloaded from stke.sciencemag.org on January 28, 2009

Probing the catalytic mechanism of action of TSC2-GAP

Unlike the "arginine finger" mechanism used by the Ras and Rho GAPs to increase the GTPase activities of their target G proteins (*30*, *45*), the TSC2-GAP homolog, Rap1GAP, uses an asparagine residue (Asn^{290}) to promote nucleotide hydrolysis in the asparagine-thumb mechanism (*46*). The analogous residue in TSC2 (Asn^{1643}) is mutated to Lys, Ile, or His in patients with tuberous sclerosis (*47*–*50*), leading to deregulation of downstream signaling through Rheb (*7*, *35*). To assess the role of Asn^{1643} in the GAP activity of TSC2, we used our NMR-based assay to analyze TSC2 proteins mutated at this position. Mutation of Asn^{1643}→Ala^{1643} in $TSC2_{1525–1742}$ completely abolished its activity as a GAP (Fig. 5C), revealing that this residue is essential to the catalytic mechanism of TSC2. To investigate the role of the functional groups of the side chain of Asn^{1643} in catalysis, this residue was mutated to Asp. Complete loss of activity in the Asn^{1643}→Asp^{1643} mutant of $TSC2_{1525–1742}$ (Fig. 5C) showed that the amide group of the side chain was essential for catalysis. Moreover, the conservative mutation Asn^{1643}→Gln^{1643}, which preserves the functional group but extends the side chain, completely eliminated activity (Fig. 5C), highlighting a strict requirement for precise positioning of the catalytic carboxamide. Finally, to determine whether TSC2 and Rheb could coordinate a RasGAP-like arginine finger mechanism, an arginine residue was incorporated in place of Asn^{1643} of TSC2, which resulted in complete loss of its functions as a GAP (Fig. 5C).

To further dissect the catalytic mechanism, TSC2-GAP activity toward various Rheb mutants was assessed. The GTPase activity of the Arg^{15}→Gly^{15} mutant of Rheb was stimulated only 3.5-fold by $TSC2_{1525–1742}$ compared to the 50-fold enhancement of the GTPase activity of WT Rheb by $TSC2_{1525–1742}$ (Fig. 5F), consistent with a previous finding that this mutant is partially resistant to the GAP activity of TSC2 (*35*). Considering that RasGAP promotes GTP hydrolysis by Ras through an arginine finger mechanism (Fig. 6B), we examined whether a more "Ras-like" Arg^{15}→Gly^{15} mutant of Rheb could be affected by a "RasGAP-like" mutant of TSC2 by measuring the GTPase activity of the Arg^{15}→Gly^{15} Rheb mutant in the presence of the arginine finger $TSC2_{1525–1742}$ GAP mutant, $TSC2_{1525–1742}$ Asn^{1643}→Arg^{1643}, and found that the rate of GTP hydrolysis [$k = (6.4 \pm 0.5) \times 10^{-4}$ min^{-1}] was similar to that of the Arg^{15}→Gly^{15} mutant of Rheb alone. Whereas we had determined that the Gln^{64}→Leu^{64} mutation did not affect the intrinsic rate of hydrolysis of GTP by Rheb (Fig. 3B), we next investigated whether Gln^{64} was involved in the GAP-catalyzed hydrolysis of GTP. Indeed, Rheb Gln^{64}→Leu^{64} was substantially less susceptible to the GAP activity of $TSC2_{1525–1742}$, exhibiting a reaction rate 60% lower than that of WT Rheb in the presence of TSC2-GAP (Fig. 5F), which suggests that Gln^{64} may play some role in the mechanism by which the GAP domain of TSC2 increases the rate of GTP hydrolysis by Rheb.

Analysis of tuberous sclerosis–associated GAP domain mutations of TSC2

Certain mutations found in *TSC2* of patients with tuberous sclerosis map to the GAP domain of TSC2 (Fig. 5A) (*48*). Although mutations of Asn^{1643} directly affect the GAP activity of TSC2 (*7*, *35*), there has been no systematic characterization of the activities of other TSC2-GAP mutants. We applied our assay to examine how six disease-associated mutations affected the ability of TSC2 to act as a GAP. We chose to examine the effects of one mutation of the catalytic Asn (Asn^{1643}→Ile^{1643}) (*50*, *51*), two mutations found within a predicted helix that contains the catalytic residue, His^{1640}→Tyr^{1640} (*52*) and Lys^{1638}→Asn^{1638} (*51*), as well as three disease-associated mutations that are predicted to map to surface-exposed regions of the GAP domain proximal to the catalytic Asn^{1643}, Glu^{1558}→Lys^{1558} (*49*, *53*), Leu^{1594}→Met^{1594} (*48*), and Asp^{1690}→Tyr^{1690} (*54*) (Fig. 5B). The quality of each TSC2-GAP mutant protein preparation was assessed from their gel-filtration chromatograms and circular dichroism (CD) spectra (fig. S7). Consistent with the loss of activity associated with four other mutations of the catalytic Asn (Fig. 5C), the $TSC2_{1525–1742}$ Asn^{1643}→Ile^{1643} mutant was inactive (Fig. 5D). Likewise, disease-associated mutations of His^{1640} and Lys^{1638}, proximal to Asn^{1643}, as well as the more distal residue Glu^{1558} each eliminated the GAP activity of TSC2 (Fig. 5D). The conservative substitution Leu^{1594}→Met^{1594} resulted in an about 80% reduction in the GAP activity of TSC2 compared to that of WT TSC2 (Fig. 5D). Conversely, the Asp^{1690}→Tyr^{1690} mutation did not impair the GAP activity of TSC2, indicating that its effect on the pathology of tuberous sclerosis likely does not involve direct modulation

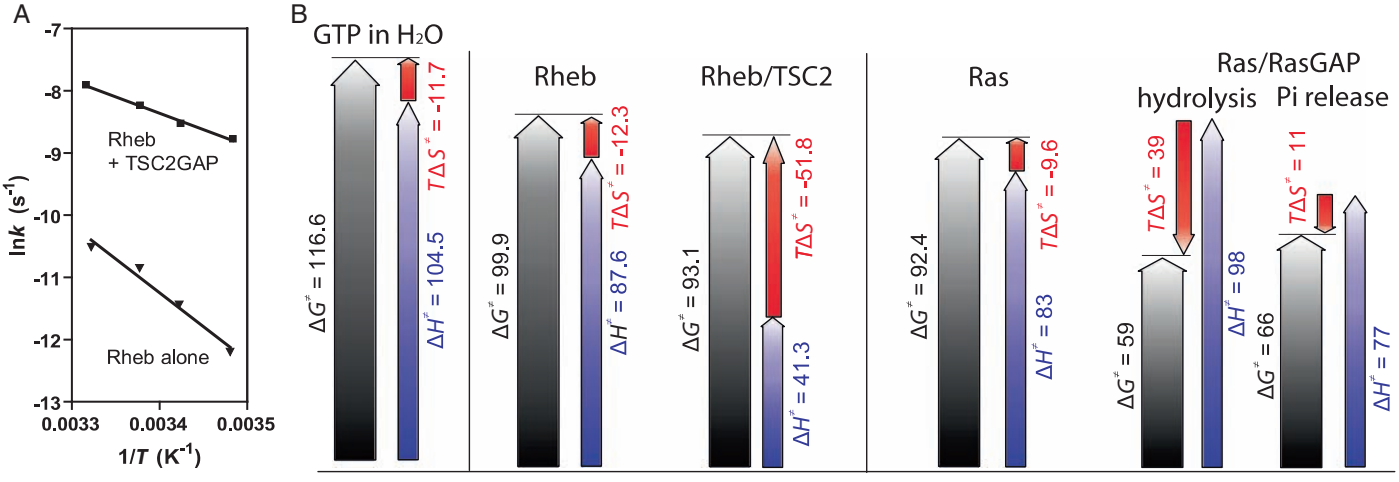

Fig. 4. Thermodynamic activation parameters for GTP hydrolysis by Rheb and the GAP domain of TSC2. (**A**) Arrhenius plots for GTP hydrolysis by Rheb alone (triangles) and in the presence of $TSC2_{1525–1742}$ (squares). Each data point represents a rate calculated from a representative GTPase assay consisting of 40 and 20 time points for Rheb alone and Rheb with TSC2, respectively. (**B**) Summary of thermodynamic activation parameters [free energy of activation ($\Delta G^{\ddagger}$), activation enthalpy ($\Delta H^{\ddagger}$), and activation entropy ($T\Delta S^{\ddagger}$) in kilojoules per mole] calculated for GTP hydrolysis by Rheb and Rheb–TSC2-GAP in this study, and, by way of comparison, for GTP alone, Ras, and Ras-RasGAP from Kötting *et al.* (*64*).

Downloaded from stke.sciencemag.org on January 28, 2009

of GAP activity. It should be noted that all of the described TSC2 mutants produced similar CD spectra, except for Glu^{1558}→Lys^{1558}, which exhibited a CD spectrum that was slightly different from that of WT TSC2 (fig S7B). The spectrum of the Glu^{1558}→Lys^{1558} mutant was likely of poor quality because it was collected at a substantially lower concentration of protein than was the case for the other TSC2 mutants, due to its limited solubility and recovery when expressed in *E. coli*. Judged by this spectrum and its reduced solubility, we cannot rule out the possibility that the lack of GAP activity of this mutant could be due to partial misfolding of the protein.

Mapping the TSC2-GAP–binding site of Rheb

The GAP activities of the assayed disease-associated mutant TSC2 proteins highlighted some of the residues required for catalysis of GTP hydrolysis, binding to Rheb, or both. To map the Rheb-binding site on the TSC2-GAP domain in more detail, we engineered several mutations of TSC2 that have not been reported in patients with tuberous sclerosis. Phe^{1666} is a conserved residue that is predicted to be spatially adjacent to the asparagine thumb and is homologous to a Rap1GAP residue implicated in binding to Rap1 (*55*). The Phe^{1666}→Ala^{1666} mutation reduced the GAP activity of the mutant protein by 95% compared to that of WT TSC2 (Fig. 5E). Asp^{1598} and Glu^{1602}, together with the disease-associated site Leu^{1594}, reside within a predicted loop homologous to a region of Rap1GAP that is involved in extensive contacts with Rap1. Surprisingly, the Asp^{1598}→Ala^{1598} and Glu^{1602}→Ala^{1602} mutants of TSC2 exhibited full GAP activity. Taken together, our systematic analysis of TSC2-GAP mutants revealed certain similarities between TSC2 and Rap1GAP within

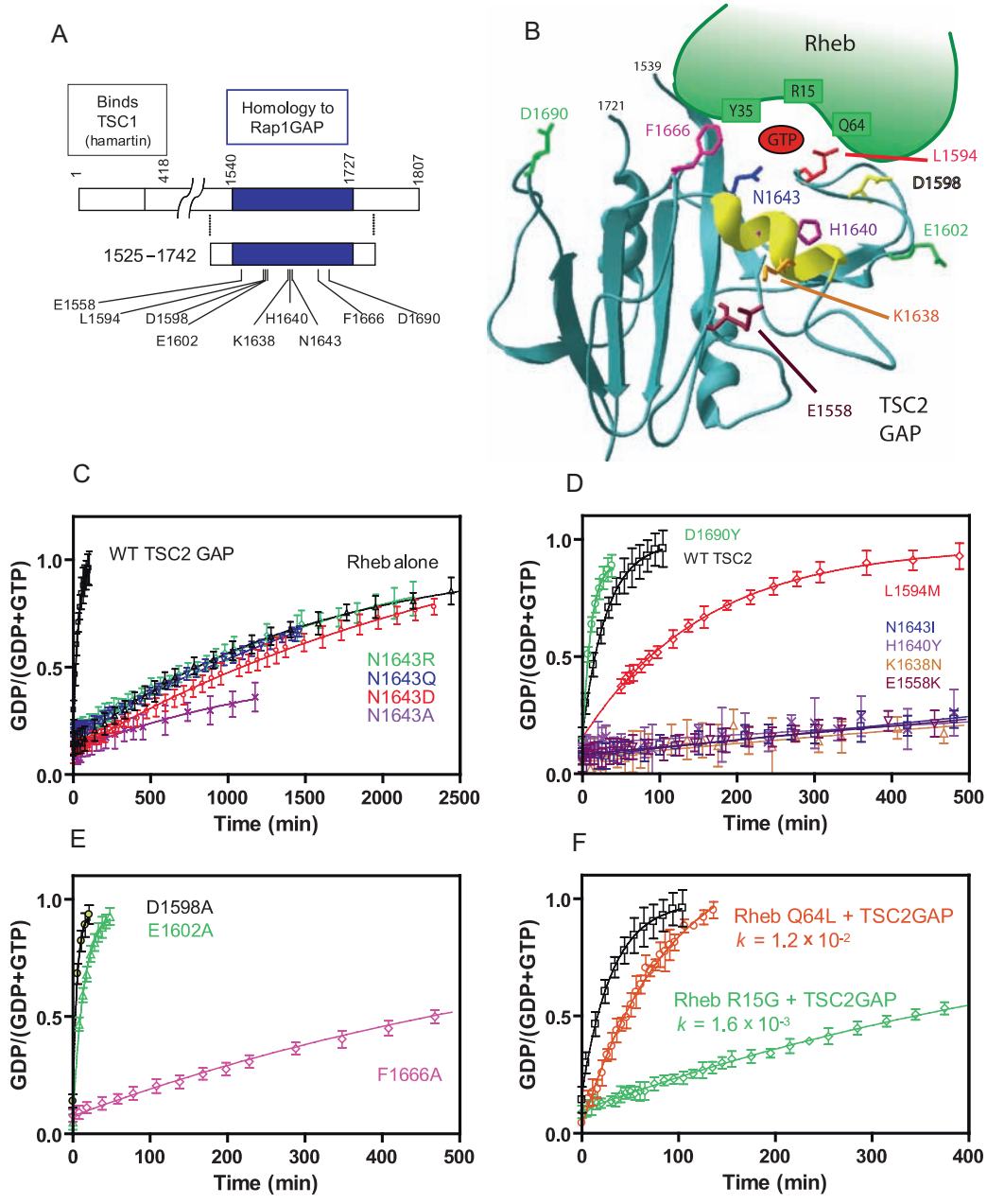

Fig. 5. Mutational analysis of the GAP activity of TSC2. (**A**) Domain map of TSC2 and the GAP domain construct indicating the positions of mutations investigated in this study. (**B**) Model of the GAP domain of TSC2 (residues 1539 to 1721) based on its homology to Rap1GAP (PDB 1SRQ) showing the position of the putative asparagine thumb, Asn^{1643}. The predicted locations of disease-associated and engineered mutations analyzed in this study are shown and the predicted helix that supports the asparagine thumb is highlighted in yellow. (**C**) GAP activity of Asn^{1643} mutants of $TSC2_{1525–1742}$ (N1643A, purple X; N1643D, red circles; N1643Q, blue inverted triangles; N1643R, green diamonds) versus WT $TSC2_{1525–1742}$ (black squares) and the intrinsic GTPase activity of Rheb alone (black triangles). (**D**) Effects of disease-associated mutations on the GAP activity of $TSC2_{1525–1742}$ (N1643I, blue squares; H1640Y, purple X; K1638N, orange diamonds; E1558K, dark red inverted triangles; L1594M, red diamonds; D1690Y, green circles; and WT $TSC2_{1525–1742}$, black squares). (**E**) Effects of engineered mutations on the GAP activity of $TSC2_{1525–1742}$ (D1598A, black circles; E1602A, green triangle; F1666A, pink diamonds). (**F**) GAP-catalyzed GTP hydrolysis by Rheb R15G (green diamonds) and Q64L (orange circles) relative to that of WT Rheb (black squares). Each curve in (C) to (F) presents the result of a representative GTPase assay in which each time point is an average of two scans and the error bars indicate the standard deviation of the fraction of GDP reported by 22 residues.

Downloaded from stke.sciencemag.org on January 28, 2009

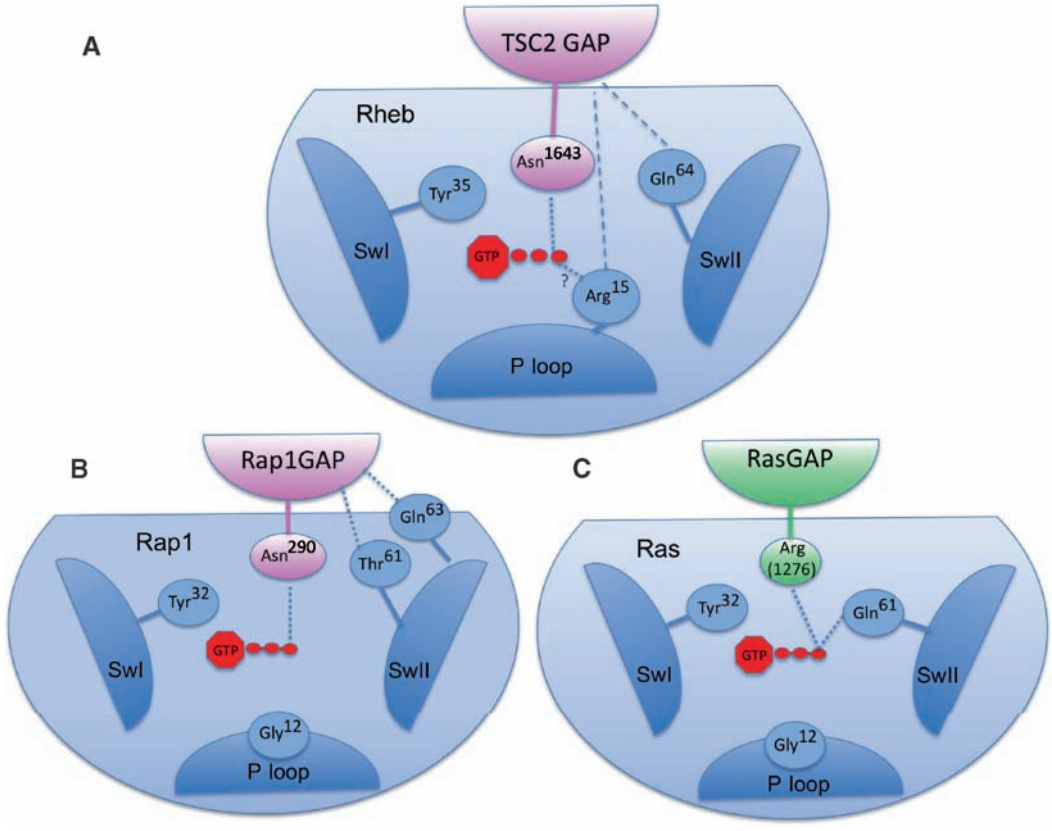

Fig. 6. Mechanisms of GAP activity. (**A**) TSC2 provides an asparagine thumb that substitutes for the Gln^{64} residue of Rheb, which is not catalytic but may form a protein-protein interaction with the GAP domain. Arg^{15}, which is not involved in the intrinsic mechanism of GTP hydrolysis, plays a role in the GAP-catalyzed reaction, either by promoting catalysis or by binding to the GAP. (**B**) Rap1 lacks the catalytic Gln^{61}, which is replaced by an asparagine thumb provided by Rap1GAP. SwI, switch I; SwII switch II. (**C**) RasGAP provides an arginine finger, which is directly involved in catalysis and stabilizes the catalytic Gln^{61} to promote activity.

the catalytic core, but key differences within the adjacent, partially conserved regions.

DISCUSSION

Based on the unique property of small GTPases that they tightly associate with both the substrate and the product of their enzymatic activity, thus assuming two distinct conformations, we have developed an NMR-based, real-time assay to analyze the intrinsic GTPase activity of Rheb and the GAP activity of TSC2. The present study is the first example of the use of two-dimensional heteronuclear NMR spectroscopy to provide a real-time comprehensive assay of the reaction kinetics of nucleotide hydrolysis by a heterotrimeric GTP-binding protein (G protein). This method relies on dynamic monitoring of changes in the chemical shifts of each amino acid residue, which are dependent on nucleotide-induced changes in the chemical environment and the structure of the protein. Among existing GTPase assays, those that use TLC or high-performance liquid chromatography (HPLC) to separate reaction products after the incubation of [β-^{32}P]GTP-loaded G protein are not consistent with determination of reaction kinetics or detection of subtle differences in GTPase activity. Although fluorescently tagged nucleotides have enabled real-time measurements of GTP hydrolysis for certain GTPases, not all G proteins are compatible with these modified nucleotides (*56*), and it cannot be predicted a priori whether a fluorescent label might interfere with the interactions between a GTPase and its regulators. The method presented here also eliminates many of the shortcomings of traditional approaches in that only well-folded protein contributes to the numeric output. Further, kinetic information is gathered for individual residues and can be directly correlated with the specific structural elements within the examined protein. Finally, our NMR-based method does not require chemical modifications of either the GTPase or the substrate, thus eliminating the biases introduced by their alterations.

Mechanistic aspects of intrinsic and TSC2-GAP–catalyzed hydrolysis of GTP by Rheb

Our work provides a quantitative measure of the rate of GTP hydrolysis by Rheb (with a half-life of ~17 hours at 19°C), which is 12- to 55-fold lower than the rates measured for various Ras isoforms (*44*, *57*–*59*). Consistently, previous end point measurements and metabolic labeling experiments have suggested that the intrinsic rate of GTP hydrolysis by Rheb is lower than that of Ras (*2*, *7*, *35*, *60*, *61*), and that Rheb isolated from cells is predominantly in the activated, GTP-bound state (*8*, *34*, *35*).

The high fidelity of our real-time, NMR-based assay allowed us to explore the activity of a minimal GAP domain of TSC2, which was previ-

Downloaded from stke.sciencemag.org on January 28, 2009

ously thought to be inactive (*35*, *46*). We found that relatively high concentrations of the GAP domain of TSC2 were required to stimulate the GTPase reaction of Rheb (200 to 400 μM [^{15}N]Rheb was used to achieve high signal-to-noise ratios in the assay and the GAP domain of TSC2 added was half of that of [^{15}N]Rheb). Under these conditions, the measured half-life of GTP was ~22 min, similar to that determined by the HPLC-based assay reported by Scrima *et al*. (*55*). In contrast, when the GAP domain of TSC2 was used at a 1:50 molar ratio relative to Rheb, there was no enhancement of the GTP hydrolysis rate by Rheb [$k = (5.2 \pm 0.6) \times 10^{-4}$ min^{-1}]. The methodology developed here lays the groundwork for the characterization of full-length TSC2 and the TSC1-TSC2 heterodimer, which may determine whether other domains in this molecular complex contribute to its affinity for Rheb or to catalysis of the GTPase activity of Rheb.

GAP domains are diverse both in their structures and in the mechanisms by which they act on their cognate G proteins (*62*). RasGAPs stabilize the Gln^{61} residue of Ras in a catalytically competent position and insert an arginine finger that interacts with the β and γ phosphates of GTP and stabilizes the transition state of the hydrolysis reaction (*30*). Although they are structurally divergent, RhoGAPs also function by a remarkably similar mechanism (*45*). The GAP domain of TSC2 is distinct from those of other GAPs, but is homologous to the catalytic domain of Rap1GAP, which uses a catalytic, asparagine thumb that appears to substitute for the catalytic glutamine that is absent in Rap1 (*46*, *55*, *63*). Our results strongly support the asparagine-thumb mechanism for the action of the GAP domain of TSC2, because mutation of Asn^{1643} to Ala, Asp, Gln, Arg, or Ile completely eliminated its GAP activity (Fig. 5, C and D). Inactivation of the GAP activity of TSC2 by the Asn^{1643}→Asp^{1643} mutation (Fig. 5C) highlighted the importance of the amide group. The complete loss of GAP activity of TSC2 after the Asn^{1643}→Gln^{1643} mutation (Fig. 5C) showed the strict requirement for the appropriate positioning of the carboxamide of the asparagine thumb, which may interact with the nucleophilic water molecule (*55*). Not surprisingly, the Asn^{1643}→Arg^{1643} mutant TSC2 protein failed to act as a GAP with either WT Rheb or the Ras-like Arg^{15}→Gly^{15} mutant of Rheb, indicating that the GAP domain of TSC2 is incompatible with an arginine finger–like catalytic mechanism.

Given the importance of the Asn^{1643} residue of TSC2 for catalysis of GTP hydrolysis by Rheb, we investigated whether this residue replaced the Gln^{64} of Rheb during GTP hydrolysis. The Gln^{64}→Leu^{64} mutant of Rheb was less sensitive than WT Rheb to the GAP activity of TSC2; however, the rate of its hydrolysis of GTP was still stimulated >20-fold by the GAP domain of TSC2 (Fig. 5F), implying that Gln^{64} of Rheb, unlike Gln^{61} of Ras, did not directly participate in GTP hydrolysis (Fig. 6). Rather, the modest reduction by this substitution of the sensitivity of the mutant protein to the GAP activity of TSC2 suggested that Gln^{64} of Rheb may contribute to proper association or complex formation with the GAP domain. Similarly, Thr^{61}, which is in the equivalent position in Rap1 to Gln^{64} of Rheb, is not catalytic, but its mutation disrupts the interaction between Rap1 and Rap1GAP (*55*, *63*).

Mutation of Gly^{12} of Ras not only impairs its intrinsic GTPase activity, but also eliminates the ability of the RasGAPs to promote GTP hydrolysis by Ras (*30–33*, *40–43*). Rheb contains an Arg in the equivalent position and our results showed that the Arg^{15}→Gly^{15} mutation had little effect on the intrinsic rate of GTP hydrolysis, but reduced the sensitivity of mutant Rheb to the GAP activity of TSC2$_{1525–1742}$ by 95% compared to that of WT Rheb. This is consistent with the possibility that Arg^{15} of Rheb is critical for the optimal interaction between Rheb and TSC2. Alternatively, the positively charged side chain of Arg^{15} may be aligned by the GAP domain of TSC2 such that it contributes to the catalytic mechanism.

Thermodynamic considerations of GTP hydrolysis by Rheb and TSC2-GAP

We studied the temperature dependence of rates of GTP hydrolysis and compared the thermodynamic activation parameters for the hydrolysis of GTP by Rheb to those previously reported for Ras. Like Ras, Rheb catalyzes GTP hydrolysis primarily by lowering the activation enthalpy, although Rheb is less potent than Ras ($\Delta\Delta H^{\ddagger} = -16.9$ kJ/mol for Rheb compared to $\Delta\Delta H^{\ddagger} = -21.7$ kJ/mol for Ras), resulting in a higher free energy of activation (99.9 kJ/mol compared to 92.4 kJ/mol) and a slower reaction rate (Fig. 4, A and B). Addition of the GAP domain of TSC2 to Rheb substantially reduced the activation enthalpy (from 87.6 to 41.3 kJ/mol), which was offset in part by a large decrease in activation entropy (from −12.3 to −51.8 kJ/mol). This is in contrast to the RasGAP neurofibromin (NF1), which drives the hydrolysis of GTP by increasing the activation entropy (−9.6 to +39 kJ/mol for the cleavage reaction) (*64*). This increase in entropy is achieved by an unconventional mechanism in which displacement of ordered water molecules from the Ras-binding pocket upon insertion of the arginine finger of NF1 provides an entropic contribution of free energy that may be used toward bond cleavage.

In contrast, our results indicate that TSC2 uses a more conventional enthalpy-driven enzymatic reaction mechanism, which typically involves stabilization of the transition state through electrostatic interactions (*65*). The thermodynamic differences between NF1 and TSC2 indicate distinct structural bases for the reactions. The asparagine thumb of TSC2 does not fill the nucleotide-binding pocket of Rheb and is unlikely to displace water molecules. Rather, formation of a structurally stabilized GAP domain-Rheb complex may be entropically unfavorable. The asparagine thumb likely contributes to the reduced activation enthalpy in a manner analogous to that of Gln^{61} of Ras; however, the large effect on $\Delta H^{\ddagger}$ suggests that auxiliary mechanisms may contribute to GTP hydrolysis. These results show that the entropic mechanism proposed for RasGAP by Kötting and co-workers (*64*) cannot be generalized for all GAPs. Further structural studies will be needed to fully elucidate the details of the catalytic activity of GAP domain of TSC2.

The effect of polymorphisms and disease-associated mutations of TSC2

Our analysis has shown that most disease-associated mutants of TSC2 affect its catalytic activity. Based on the shared asparagine thumb–based catalytic mechanism and sequence homology between Rap1GAP and TSC2, we analyzed the GAP activity of a series of tuberous sclerosis–associated mutations in TSC2 that were predicted to occur at surface residues (Fig. 5B). Consistent with our analysis of other mutations of the asparagine thumb (Fig. 5C), the disease mutation Asn^{1643}→Ile^{1643} (*50*, *51*) eliminated the activity of the GAP domain of the mutant TSC2, which strongly suggested that the inability to inactivate Rheb underlies the pathogenesis of this mutation, as is likely the case with the other disease-associated mutations at this position: Asn^{1643}→His^{1643} (*49*) and Asn^{1643}→Lys^{1643} (*48*).

The catalytic Asn of Rap1GAP is situated at the C terminus of an eight-residue helix (*46*), which is conserved in TSC2. We found that tuberous sclerosis–associated mutations in two invariant residues within this helix, His^{1640}→Tyr^{1640} (*52*) and Lys^{1638}→Asn^{1638} [Leiden Open Variation Database (LOVD)], eliminated GAP activity (Fig. 5D). The solved structures of Rap1GAP (*46*, *55*) suggest that these residues, which correspond to His^{287} and Lys^{285} in Rap1GAP, respectively, are important for proper positioning of the helix, and thus of the catalytic Asn of TSC2, for catalysis. The Lys^{285} residue of Rap1GAP forms an intramolecular salt bridge with the invariant Glu^{207}, and mutation of either of these residues profoundly impairs the activity of Rap1GAP (*46*, *55*, *66*). Likewise, a tuberous sclerosis–associated TSC2 mutant, Glu^{1558}→Lys^{1558}

Downloaded from stke.sciencemag.org on January 28, 2009

(*49*, *53*), which is homologous to Glu^{207} of Rap1GAP, abolished its GAP activity (Fig. 5D), possibly by destabilizing the structure of the GAP domain.

The complete loss of activity associated with these mutations is likely due directly to disrupted catalytic function. To identify residues of the GAP domain of TSC2 involved in binding to Rheb, we analyzed disease-associated mutations and engineered mutations of residues predicted to be proximal to the catalytic residue in the three-dimensional structure of TSC2. Phe^{1666} of TSC2 is conserved and equivalent to Phe^{313} of Rap1GAP, which forms part of a hydrophobic binding site for Rap1 beside the asparagine thumb. The mutation Phe^{1666}→Ala^{1666} reduced the GAP activity of TSC2 by 95% compared to that of WT TSC2 (Fig. 5E), suggesting that a hydrophobic patch similar to that of Rap1GAP plays a role in the docking of Rheb with TSC2. On the other side of the asparagine thumb, a long loop in Rap1GAP is involved in extensive protein-protein contacts with Rap1 (*55*), and several disease-associated mutations have been found in the corresponding region of TSC2, including Leu^{1594}→Met^{1594} (*48*), Gly^{1595}→Arg^{1595} (LOVD), and Leu^{1597}→Pro^{1597} (*49*). Surprisingly, a conservative Leu^{1594}→Met^{1594} substitution at this position substantially reduced the GAP activity of TSC2 (Fig. 5D). Because fully active Rap1GAP contains a divergent Arg at the position homologous to the Leu^{1594} of TSC2, this implicates this region in determining the specificities of these GAPs toward their cognate GTPases. To examine the role of a conserved residue within this loop, we designed a mutation of a strictly conserved residue, Asp^{1598}, which is homologous to Asp^{244} of Rap1GAP, which appears to be important for binding to Rap1. Nevertheless, the Asp^{1598}→Ala^{1598} mutation had no effect on the GAP activity of TSC2, revealing further differences between Rap1 and TSC2 in this region. Likewise, mutation of TSC2 Glu^{1602} to Ala did not reduce its GAP activity. Finally, we found that the disease-associated TSC2 mutation of Asp^{1690}, a residue found variant in independent cohorts of patients with tuberous sclerosis (LOVD), to Tyr surprisingly had no effect on GAP activity. Participation of this residue in the pathology of tuberous sclerosis is likely mediated by another aspect of TSC2 function, such as its interaction with TSC1, its intracellular trafficking, its stability, or its susceptibility to regulatory posttranslational modifications such as phosphorylation.

Implications for the analysis of other GTPases

The real-time, NMR-based method described here can, in principle, be applied to any G protein, as well as to the analysis of the regulatory effect of their cognate GAPs and GEFs. In the case of Rheb, considering its relatively low intrinsic GTPase activity, the frequency and the duration of collection of each HSQC spectrum was not a factor in deriving the rate of GTP hydrolysis. However, for the analysis of more efficient GTPases, such as Ras and Rho, the temporal resolution of data collection can be substantially improved on by the recently developed band-selective optimized flip-angle short transient (SOFAST) NMR pulse sequence, which facilitates collection of two-dimensional heteronuclear multiple quantum coherence (HMQC) spectra with a temporal resolution of a few seconds (*67*). We used this methodology to perform a real-time, NMR-based assay of GAP activity in which each spectrum was collected in 30 s (fig. S8). The rate of this TSC2-GAP–catalyzed reaction is comparable to the intrinsic GTPase rate of Ras, and >70 data points were obtained to monitor the reaction. Capturing the extremely rapid RasGAP-catalyzed reactions would be challenging, but might be accomplished by titration of the concentration of the GAP protein to achieve a suitable reaction rate. Another challenge to studying highly active GTPases is in obtaining fully GTP-loaded protein preparations. This could be overcome through the use of photocaged GTP analogs, which remain stable in complex with the G protein until their activation by a pulse of light (*68*). Finally, although the current protocol requires substantial quantities of protein (500 μl of sample at a concentration of ≥200 μM, or >2 mg per assay), we have obtained reasonable results with as little as 30 μl of sample at a concentration of ≤200 μM (~100 μg total protein) with a recently developed 1.7-mm microcryoprobe (Bruker Biospin) (fig. S9). Despite these challenges, real-time NMR enables the acquisition of temporally resolved, structure-specific data with nonradioactive, unmodified, natural nucleotides, which should provide further mechanistic detail and a deeper understanding of the nucleotide catalysis reactions of many small GTPases.

MATERIALS AND METHODS

Sample preparation and resonance assignments

The G domain of Rheb (residues 1 to 169, with the C-terminal hypervariable region and the CAAX box truncated) was expressed as a glutathione-*S*-transferase (GST) fusion protein from PGEX2T in the *E. coli* strain BL21 DE3 Codon+ by induction with 0.2 mM isopropyl-β-D-thiogalactopyranoside at 15°C overnight and enriched by binding to a glutathione-Sepharose resin. Rheb was cleaved from GST on the resin with thrombin and further purified by gel-filtration chromatography (S-75). Recombinant Rheb expressed in *E. coli* was purified primarily in the GDP-bound form. GMPPNP-bound Rheb was prepared by adding an excess of this nonhydrolyzable GTP analog in the presence of EDTA to decrease the affinity of GDP and calf instestinal alkaline phosphatase to degrade GDP (*39*). [^{13}C-^{15}N]Rheb and deuterated [^{13}C-^{15}N]Rheb were produced in M9 media supplemented with [^{13}C]glucose and [^{15}N]ammonium chloride, and triple-resonance experiments were performed to assign backbone resonances (see Supplementary Methods). For GTPase assays, [^{15}N]Rheb was loaded with GTP by incubation with a 10-fold excess of GTP in the presence of EDTA. After replenishing Mg^{2+}, excess nucleotide and EDTA were removed with a desalting column and the HSQC spectra were collected as soon as possible.

NMR-based GTPase assay

^{1}H-^{15}N sensitivity–enhanced HSQC spectra (two scans) were collected on a Bruker Advance II 800-MHz spectrometer equipped with a 5-mm TCI CryoProbe. The concentration of Rheb was 0.2 to 0.5 mM, and acquisition of each spectrum required 5 min. NMR spectra were processed and analyzed with NMRpipe (*69*). Cross peaks were picked and assigned in the reference spectra to create Rheb-GTP (first spectrum) and Rheb-GDP (last spectrum); peak lists and peak heights were extracted for each spectrum. The fraction of Rheb in the GDP-bound form [$I_{GDP}/(I_{GDP} + I_{GTP})$] was calculated from the peak intensities (I) of 22 reporter residues, plotted against time, and fit to a one-phase exponential decay curve. A construct encoding residues 1525 to 1742 of TSC2 was cloned into pGEX2T, expressed in LB medium and purified as described for Rheb. A homology model of the GAP domain of TSC2 including residues 1539 to 1721 was constructed with SWISS-MODEL (*70*) with Rap1GAP (PDB 1SRQ) as a template. To assay GTP hydrolysis in the presence of the GAP domain, a reference spectrum of GTP-loaded Rheb was collected; a small volume of highly concentrated GAP in NMR buffer was added (in a 1:2 molar ratio) and a series of spectra were collected, initially at 5-min intervals. Mutants of Rheb and TSC2 were generated with Quikchange (Stratagene) and sequences were confirmed by DNA sequencing.

Thermodynamic activation parameters for GTPase activity of Rheb alone and with TSC2

To measure the thermodynamic activation parameters for GTP hydrolysis by Rheb alone and for the TSC2-GAP–catalyzed reaction, the

Downloaded from stke.sciencemag.org on January 28, 2009

NMR-based GTPase assay was performed at four different temperatures (287, 292, 296, and 301.5 K). $TSC2_{1525–1742}$ was added to Rheb at a molar ratio of 1:7. Arrhenius plots were constructed by plotting $\ln(k)$ as a function of $1/T$ and were then used to calculate activation energy (E_a), activation entropy ($\Delta S^{\ddagger}$), activation enthalpy ($\Delta H^{\ddagger}$), and free energy of activation ($\Delta G^{\ddagger}$).

SUPPLEMENTARY MATERIALS

www.sciencesignaling.org/cgi/content/full/2/55/ra3/DC1
Methods
Fig. S1. Role of Rheb in mTOR signaling.
Fig. S2. Spectra of Rheb-GDP and Rheb-GMPPNP.
Fig. S3. Secondary structure and chemical shift index analysis.
Fig. S4. Preparation of Rheb-GTP for GTPase assay.
Fig. S5. Time course of GTP hydrolysis of Rheb-GTP.
Fig. S6. Analysis of Rheb-GTP and Rheb-GDP during GTP hydrolysis.
Fig. S7. Circular dichroism spectra of WT $TSC2_{1225–1742}$ and its variants.
Fig. S8. Further development of real-time NMR method to increase temporal resolution.
Fig. S9. Further development of real-time NMR method to decrease sample requirement.
References

REFERENCES AND NOTES

1. G. W. Reuther, C. J. Der, The Ras branch of small GTPases: Ras family members don't fall far from the tree. *Curr. Opin. Cell Biol.* **12**, 157–165 (2000).
2. K. Yamagata, L. K. Sanders, W. E. Kaufmann, W. Yee, C. A. Barnes, D. Nathans, P. F. Worley, *rheb*, a growth factor– and synaptic activity–regulated gene, encodes a novel Ras-related protein. *J. Biol. Chem.* **269**, 16333–16339 (1994).
3. A. P. Tabancay Jr., C. L. Gau, I. M. Machado, E. J. Uhlmann, D. H. Gutmann, L. Guo, F. Tamanoi, Identification of dominant negative mutants of Rheb GTPase and their use to implicate the involvement of human Rheb in the activation of p70S6K. *J. Biol. Chem.* **278**, 39921–39930 (2003).
4. H. Stocker, T. Radimerski, B. Schindelholz, F. Wittwer, P. Belawat, P. Daram, S. Breuer, G. Thomas, E. Hafen, Rheb is an essential regulator of S6K in controlling cell growth in *Drosophila*. *Nat. Cell Biol.* **5**, 559–565 (2003).
5. L. J. Saucedo, X. Gao, D. A. Chiarelli, L. Li, D. Pan, B. A. Edgar, Rheb promotes cell growth as a component of the insulin/TOR signalling network. *Nat. Cell Biol.* **5**, 566–571 (2003).
6. A. Garami, F. J. Zwartkruis, T. Nobukuni, M. Joaquin, M. Roccio, H. Stocker, S. C. Kozma, E. Hafen, J. L. Bos, G. Thomas, Insulin activation of Rheb, a mediator of mTOR/S6K/4E-BP signaling, is inhibited by TSC1 and 2. *Mol. Cell* **11**, 1457–1466 (2003).
7. Y. Zhang, X. Gao, L. J. Saucedo, B. Ru, B. A. Edgar, D. Pan, Rheb is a direct target of the tuberous sclerosis tumour suppressor proteins. *Nat. Cell Biol.* **5**, 578–581 (2003).
8. K. Inoki, Y. Li, T. Xu, K. L. Guan, Rheb GTPase is a direct target of TSC2 GAP activity and regulates mTOR signaling. *Genes Dev.* **17**, 1829–1834 (2003).
9. P. B. Crino, K. L. Nathanson, E. P. Henske, The tuberous sclerosis complex. *N. Engl. J. Med.* **355**, 1345–1356 (2006).
10. J. Huang, B. D. Manning, The TSC1-TSC2 complex: A molecular switchboard controlling cell growth. *Biochem. J.* **412**, 179–190 (2008).
11. D. J. Kwiatkowski, B. D. Manning, Tuberous sclerosis: A GAP at the crossroads of multiple signaling pathways. *Hum. Mol. Genet.* **14** (Spec No. 2), R251–R258 (2005).
12. L. Beretta, A. C. Gingras, Y. V. Svitkin, M. N. Hall, N. Sonenberg, Rapamycin blocks the phosphorylation of 4E-BP1 and inhibits cap-dependent initiation of translation. *EMBO J.* **15**, 658–664 (1996).
13. A. C. Gingras, B. Raught, N. Sonenberg, Regulation of translation initiation by FRAP/mTOR. *Genes Dev.* **15**, 807–826 (2001).
14. I. Ruvinsky, O. Meyuhas, Ribosomal protein S6 phosphorylation: From protein synthesis to cell size. *Trends Biochem. Sci.* **31**, 342–348 (2006).
15. Y. Yu, S. Li, X. Xu, Y. Li, K. Guan, E. Arnold, J. Ding, Structural basis for the unique biological function of small GTPase RHEB. *J. Biol. Chem.* **280**, 17093–17100 (2005).
16. M. van Slegtenhorst, M. Nellist, B. Nagelkerken, J. Cheadle, R. Snell, A. van den Ouweland, A. Reuser, J. Sampson, D. Halley, P. van der Sluijs, Interaction between hamartin and tuberin, the TSC1 and TSC2 gene products. *Hum. Mol. Genet.* **7**, 1053–1057 (1998).
17. M. P. DeYoung, P. Horak, A. Sofer, D. Sgroi, L. W. Ellisen, Hypoxia regulates TSC1/2-mTOR signaling and tumor suppression through REDD1-mediated 14-3-3 shuttling. *Genes Dev.* **22**, 239–251 (2008).
18. K. Inoki, Y. Li, T. Zhu, J. Wu, K. L. Guan, TSC2 is phosphorylated and inhibited by Akt and suppresses mTOR signalling. *Nat. Cell Biol.* **4**, 648–657 (2002).
19. B. D. Manning, A. R. Tee, M. N. Logsdon, J. Blenis, L. C. Cantley, Identification of the tuberous sclerosis complex–2 tumor suppressor gene product tuberin as a target of the phosphoinositide 3-kinase/Akt pathway. *Mol. Cell* **10**, 151–162 (2002).
20. J. Avruch, K. Hara, Y. Lin, M. Liu, X. Long, S. Ortiz-Vega, K. Yonezawa, Insulin and amino-acid regulation of mTOR signaling and kinase activity through the Rheb GTPase. *Oncogene* **25**, 6361–6372 (2006).
21. K. Inoki, T. Zhu, K. L. Guan, TSC2 mediates cellular energy response to control cell growth and survival. *Cell* **115**, 577–590 (2003).
22. H. C. Dan, M. Sun, L. Yang, R. I. Feldman, X. M. Sui, C. C. Ou, M. Nellist, R. S. Yeung, D. J. Halley, S. V. Nicosia, W. J. Pledger, J. Q. Cheng, Phosphatidylinositol 3-kinase/Akt pathway regulates tuberous sclerosis tumor suppressor complex by phosphorylation of tuberin. *J. Biol. Chem.* **277**, 35364–35370 (2002).
23. L. Ma, Z. Chen, H. Erdjument-Bromage, P. Tempst, P. P. Pandolfi, Phosphorylation and functional inactivation of TSC2 by Erk implications for tuberous sclerosis and cancer pathogenesis. *Cell* **121**, 179–193 (2005).
24. P. P. Roux, B. A. Ballif, R. Anjum, S. P. Gygi, J. Blenis, Tumor-promoting phorbol esters and activated Ras inactivate the tuberous sclerosis tumor suppressor complex via p90 ribosomal S6 kinase. *Proc. Natl. Acad. Sci. U.S.A.* **101**, 13489–13494 (2004).
25. A. Astrinidis, W. Senapedis, T. R. Coleman, E. P. Henske, Cell cycle–regulated phosphorylation of hamartin, the product of the tuberous sclerosis complex 1 gene, by cyclin-dependent kinase 1/cyclin B. *J. Biol. Chem.* **278**, 51372–51379 (2003).
26. D. F. Lee, H. P. Kuo, C. T. Chen, J. M. Hsu, C. K. Chou, Y. Wei, H. L. Sun, L. Y. Li, B. Ping, W. C. Huang, X. He, J. Y. Hung, C. C. Lai, Q. Ding, J. L. Su, J. Y. Yang, A. A. Sahin, G. N. Hortobagyi, F. J. Tsai, C. H. Tsai, M. C. Hung, IKKβ suppression of TSC1 links inflammation and tumor angiogenesis via the mTOR pathway. *Cell* **130**, 440–455 (2007).
27. K. Inoki, H. Ouyang, T. Zhu, C. Lindvall, Y. Wang, X. Zhang, Q. Yang, C. Bennett, Y. Harada, K. Stankunas, C. Y. Wang, X. He, O. A. MacDougald, M. You, B. O. Williams, K. L. Guan, TSC2 integrates Wnt and energy signals via a coordinated phosphorylation by AMPK and GSK3 to regulate cell growth. *Cell* **126**, 955–968 (2006).
28. J. Brugarolas, K. Lei, R. L. Hurley, B. D. Manning, J. H. Reiling, E. Hafen, L. A. Witters, L. W. Ellisen, W. G. Kaelin Jr., Regulation of mTOR function in response to hypoxia by REDD1 and the TSC1/TSC2 tumor suppressor complex. *Genes Dev.* **18**, 2893–2904 (2004).
29. H. Maruta, J. Holden, A. Sizeland, G. D'Abaco, The residues of Ras and Rap proteins that determine their GAP specificities. *J. Biol. Chem.* **266**, 11661–11668 (1991).
30. K. Scheffzek, M. R. Ahmadian, W. Kabsch, L. Wiesmuller, A. Lautwein, F. Schmitz, A. Wittinghofer, The Ras-RasGAP complex: Structural basis for GTPase activation and its loss in oncogenic Ras mutants. *Science* **277**, 333–338 (1997).
31. M. Barbacid, *ras* genes. *Annu. Rev. Biochem.* **56**, 779–827 (1987).
32. U. Krengel, I. Schlichting, A. Scherer, R. Schumann, M. Frech, J. John, W. Kabsch, E. F. Pai, A. Wittinghofer, Three-dimensional structures of H-*ras* p21 mutants: Molecular basis for their inability to function as signal switch molecules. *Cell* **62**, 539–548 (1990).
33. C. Calés, J. F. Hancock, C. J. Marshall, A. Hall, The cytoplasmic protein GAP is implicated as the target for regulation by the *ras* gene product. *Nature* **332**, 548–551 (1988).
34. E. Im, F. C. von Lintig, J. Chen, S. Zhuang, W. Qui, S. Chowdhury, P. F. Worley, G. R. Boss, R. B. Pilz, Rheb is in a high activation state and inhibits B-Raf kinase in mammalian cells. *Oncogene* **21**, 6356–6365 (2002).
35. Y. Li, K. Inoki, K. L. Guan, Biochemical and functional characterizations of small GTPase Rheb and TSC2 GAP activity. *Mol. Cell. Biol.* **24**, 7965–7975 (2004).
36. M. Sattler, J. Schleucher, C. Griesinger, Heteronuclear multidimensional NMR experiments for the structure determination of proteins in solution employing pulsed field gradients. *Prog. Nucl. Magn. Reson. Spectrosc.* **34**, 93–158 (1999).
37. Y. Ito, K. Yamasaki, J. Iwahara, T. Terada, A. Kamiya, M. Shirouzu, Y. Muto, G. Kawai, S. Yokoyama, E. D. Laue, M. Walchli, T. Shibata, S. Nishimura, T. Miyazawa, Regional polysterism in the GTP-bound form of the human c-Ha-Ras protein. *Biochemistry* **36**, 9109–9119 (1997).
38. D. S. Wishart, B. D. Sykes, F. M. Richards, The chemical shift index: A fast and simple method for the assignment of protein secondary structure through NMR spectroscopy. *Biochemistry* **31**, 1647–1651 (1992).
39. J. John, R. Sohmen, J. Feuerstein, R. Linke, A. Wittinghofer, R. S. Goody, Kinetics of interaction of nucleotides with nucleotide-free H-*ras* p21. *Biochemistry* **29**, 6058–6065 (1990).
40. P. H. Seeburg, W. W. Colby, D. J. Capon, D. V. Goeddel, A. D. Levinson, Biological properties of human c-Ha-*ras*1 genes mutated at codon 12. *Nature* **312**, 71–75 (1984).
41. P. Gideon, J. John, M. Frech, A. Lautwein, R. Clark, J. E. Scheffler, A. Wittinghofer, Mutational and kinetic analyses of the GTPase-activating protein (GAP)-p21 interaction: The C-terminal domain of GAP is not sufficient for full activity. *Mol. Cell. Biol.* **12**, 2050–2056 (1992).
42. M. R. Ahmadian, T. Zor, D. Vogt, W. Kabsch, Z. Selinger, A. Wittinghofer, K. Scheffzek, Guanosine triphosphatase stimulation of oncogenic Ras mutants. *Proc. Natl. Acad. Sci. U.S.A.* **96**, 7065–7070 (1999).
43. J. John, M. Frech, A. Wittinghofer, Biochemical properties of Ha-ras encoded p21 mutants and mechanism of the autophosphorylation reaction. *J. Biol. Chem.* **263**, 11792–11799 (1988).
44. C. Kötting, K. Gerwert, Time-resolved FTIR studies provide activation free energy, activation enthalpy and activation entropy for GTPase reactions. *Chem. Phys.* **307**, 227–232 (2004).

Downloaded from stke.sciencemag.org on January 28, 2009

45. K. Rittinger, P. A. Walker, J. F. Eccleston, S. J. Smerdon, S. J. Gamblin, Structure at 1.65 Å of RhoA and its GTPase-activating protein in complex with a transition-state analogue. *Nature* **389**, 758–762 (1997).
46. O. Daumke, M. Weyand, P. P. Chakrabarti, I. R. Vetter, A. Wittinghofer, The GTPase-activating protein Rap1GAP uses a catalytic asparagine. *Nature* **429**, 197–201 (2004).
47. A. C. Jones, M. M. Shyamsundar, M. W. Thomas, J. Maynard, S. Idziaszczyk, S. Tomkins, J. R. Sampson, J. P. Cheadle, Comprehensive mutation analysis of TSC1 and TSC2-and phenotypic correlations in 150 families with tuberous sclerosis. *Am. J. Hum. Genet.* **64**, 1305–1315 (1999).
48. M. M. Maheshwar, J. P. Cheadle, A. C. Jones, J. Myring, A. E. Fryer, P. C. Harris, J. R. Sampson, The GAP-related domain of tuberin, the product of the TSC2 gene, is a target for missense mutations in tuberous sclerosis. *Hum. Mol. Genet.* **6**, 1991–1996 (1997).
49. S. L. Dabora, S. Jozwiak, D. N. Franz, P. S. Roberts, A. Nieto, J. Chung, Y. S. Choy, M. P. Reeve, E. Thiele, J. C. Egelhoff, J. Kasprzyk-Obara, D. Domanska-Pakiela, D. J. Kwiatkowski, Mutational analysis in a cohort of 224 tuberous sclerosis patients indicates increased severity of TSC2, compared with TSC1, disease in multiple organs. *Am. J. Hum. Genet.* **68**, 64–80 (2001).
50. K. S. Au, J. A. Rodriguez, J. L. Finch, K. A. Volcik, E. S. Roach, M. R. Delgado, E. Rodriguez Jr., H. Northrup, Germ-line mutational analysis of the TSC2 gene in 90 tuberous-sclerosis patients. *Am. J. Hum. Genet.* **62**, 286–294 (1998).
51. K. S. Au, A. T. Williams, E. S. Roach, L. Batchelor, S. P. Sparagana, M. R. Delgado, J. W. Wheless, J. E. Baumgartner, B. B. Roa, C. M. Wilson, T. K. Smith-Knuppel, M. Y. Cheung, V. H. Whittemore, T. M. King, H. Northrup, Genotype/phenotype correlation in 325 individuals referred for a diagnosis of tuberous sclerosis complex in the United States. *Genet. Med.* **9**, 88–100 (2007).
52. N. Langkau, N. Martin, R. Brandt, K. Zugge, S. Quast, G. Wiegele, A. Jauch, M. Rehm, A. Kuhl, M. Mack-Vetter, L. B. Zimmerhackl, B. Janssen, TSC1 and TSC2 mutations in tuberous sclerosis, the associated phenotypes and a model to explain observed TSC1/TSC2 frequency ratios. *Eur. J. Pediatr.* **161**, 393–402 (2002).
53. N. D. Rendtorff, B. Bjerregaard, M. Frodin, S. Kjaergaard, H. Hove, F. Skovby, K. Brondum-Nielsen, M. Schwartz, Analysis of 65 tuberous sclerosis complex (TSC) patients by TSC2 DGGE, TSC1/TSC2 MLPA, and TSC1 long-range PCR sequencing, and report of 28 novel mutations. *Hum. Mutat.* **26**, 374–383 (2005).
54. R. L. Beauchamp, A. Banwell, P. McNamara, M. Jacobsen, E. Higgins, H. Northrup, P. Short, K. Sims, L. Ozelius, V. Ramesh, Exon scanning of the entire TSC2 gene for germline mutations in 40 unrelated patients with tuberous sclerosis. *Hum. Mutat.* **12**, 408–416 (1998).
55. A. Scrima, C. Thomas, D. Deaconescu, A. Wittinghofer, The Rap-RapGAP complex: GTP hydrolysis without catalytic glutamine and arginine residues. *EMBO J.* **27**, 1145–1153 (2008).
56. A. Eberth, R. Dvorsky, C. F. Becker, A. Beste, R. S. Goody, M. R. Ahmadian, Monitoring the real-time kinetics of the hydrolysis reaction of guanine nucleotide–binding proteins. *Biol. Chem.* **386**, 1105–1114 (2005).
57. J. John, I. Schlichting, E. Schiltz, P. Rosch, A. Wittinghofer, C-terminal truncation of p21H preserves crucial kinetic and structural properties. *J. Biol. Chem.* **264**, 13086–13092 (1989).
58. A. Shutes, C. J. Der, Real-time in vitro measurement of intrinsic and Ras GAP-mediated GTP hydrolysis. *Methods Enzymol.* **407**, 9–22 (2006).
59. A. Löw, M. Sprinzl, S. Limmer, Nucleotide binding and GTP hydrolysis by the 21-kDa product of the c-H-*ras* gene as monitored by proton-NMR spectroscopy. *Eur. J. Biochem.* **213**, 781–788 (1993).
60. Y. Li, K. Inoki, H. Vikis, K. L. Guan, Measurements of TSC2 GAP activity toward Rheb. *Methods Enzymol.* **407**, 46–54 (2006).
61. A. R. Tee, B. D. Manning, P. P. Roux, L. C. Cantley, J. Blenis, Tuberous sclerosis complex gene products, Tuberin and Hamartin, control mTOR signaling by acting as a GTPase-activating protein complex toward Rheb. *Curr. Biol.* **13**, 1259–1268 (2003).
62. K. Scheffzek, M. R. Ahmadian, GTPase activating proteins: Structural and functional insights 18 years after discovery. *Cell. Mol. Life Sci.* **62**, 3014–3038 (2005).
63. P. P. Chakrabarti, O. Daumke, Y. Suveyzdis, C. Kotting, K. Gerwert, A. Wittinghofer, Insight into catalysis of a unique GTPase reaction by a combined biochemical and FTIR approach. *J. Mol. Biol.* **367**, 983–995 (2007).
64. C. Kötting, A. Kallenbach, Y. Suveyzdis, A. Wittinghofer, K. Gerwert, The GAP arginine finger movement into the catalytic site of Ras increases the activation entropy. *Proc. Natl. Acad. Sci. U.S.A.* **105**, 6260–6265 (2008).
65. A. Warshel, P. K. Sharma, M. Kato, Y. Xiang, H. Liu, M. H. Olsson, Electrostatic basis for enzyme catalysis. *Chem. Rev.* **106**, 3210–3235 (2006).
66. T. Brinkmann, O. Daumke, U. Herbrand, D. Kuhlmann, P. Stege, M. R. Ahmadian, A. Wittinghofer, Rap-specific GTPase activating protein follows an alternative mechanism. *J. Biol. Chem.* **277**, 12525–12531 (2002).
67. P. Schanda, V. Forge, B. Brutscher, Protein folding and unfolding studied at atomic resolution by fast two-dimensional NMR spectroscopy. *Proc. Natl. Acad. Sci. U.S.A.* **104**, 11257–11262 (2007).
68. I. Schlichting, G. Rapp, J. John, A. Wittinghofer, E. F. Pai, R. S. Goody, Biochemical and crystallographic characterization of a complex of c-Ha-*ras* p21 and caged GTP with flash photolysis. *Proc. Natl. Acad. Sci. U.S.A.* **86**, 7687–7690 (1989).
69. F. Delaglio, S. Grzesiek, G. W. Vuister, G. Zhu, J. Pfeifer, A. Bax, NMRPipe: A multidimensional spectral processing system based on UNIX pipes. *J. Biomol. NMR* **6**, 277–293 (1995).
70. T. Schwede, J. Kopp, N. Guex, M. C. Peitsch, SWISS-MODEL: An automated protein homology-modeling server. *Nucleic Acids Res.* **31**, 3381–3385 (2003).
71. This work was supported by a grant from the Cancer Research Society (Canada) and a U.S. Department of Defense Tuberous Sclerosis Complex Research Program Award to V.S. A grant from the Canada Foundation for Innovation funded the 800-MHz NMR spectrometer. C.B.M. was supported by a postdoctoral fellowship from the Canadian Institutes of Health Research. M.I. and V.S. hold Canada Research Chairs and V.S. holds an Early Researcher Award from the Government of Ontario. We thank D. Moskau (Bruker Biospin AG, Fällanden, Switzerland) for data collection with a 1.7-mm cryoprobe and M. Yang, K. Su, and C. Fisher for assistance in the laboratory.

Submitted 8 September 2008
Accepted 24 December 2008
Final Publication 27 January 2009
10.1126/scisignal.2000029
Citation: C. B. Marshall, J. Ho, C. Buerger, M. J. Plevin, G.-Y. Li, Z. Li, M. Ikura, V. Stambolic, Characterization of the intrinsic and TSC2-GAP–regulated GTPase activity of Rheb by real-time NMR. *Sci. Signal.* **2**, ra3 (2009).

Downloaded from stke.sciencemag.org on January 28, 2009

Supplemental Material can be found at:
http://www.jbc.org/content/suppl/2009/12/14/C109.064766.DC1.html

THE JOURNAL OF BIOLOGICAL CHEMISTRY VOL. 285, NO. 8, pp. 5132–5136, February 19, 2010
© 2010 by The American Society for Biochemistry and Molecular Biology, Inc. Printed in the U.S.A.

Real-time NMR Study of Three Small GTPases Reveals That Fluorescent 2′(3′)-*O*-(*N*-Methylanthraniloyl)-tagged Nucleotides Alter Hydrolysis and Exchange Kinetics*[S]

Received for publication, September 10, 2009, and in revised form, November 20, 2009
Published, JBC Papers in Press, December 14, 2009, DOI 10.1074/jbc.C109.064766

Mohammad T. Mazhab-Jafari[‡§], Christopher B. Marshall[‡§1], Matthew Smith[‡§], Geneviève M. C. Gasmi-Seabrook[‡§], Vuk Stambolic[‡§2], Robert Rottapel[§¶], Benjamin G. Neel[§¶3], and Mitsuhiko Ikura[‡§3,4]

From the [‡]Division of Signaling Biology and the [¶]Division of Stem Cell and Developmental Biology, Ontario Cancer Institute, University Health Network, Toronto, Ontario M5G 1L7 and the [§]Department of Medical Biophysics, University of Toronto, Toronto, Ontario M5G 2M9, Canada

The Ras family of small GTPases control diverse signaling pathways through a conserved "switch" mechanism, which is turned on by binding of GTP and turned off by GTP hydrolysis to GDP. Full understanding of GTPase switch functions requires reliable, quantitative assays for nucleotide binding and hydrolysis. Fluorescently labeled guanine nucleotides, such as 2′(3′)-*O*-(*N*-methylanthraniloyl) (mant)-substituted GTP and GDP analogs, have been widely used to investigate the molecular properties of small GTPases, including Ras and Rho. Using a recently developed NMR method, we show that the kinetics of nucleotide hydrolysis and exchange by three small GTPases, alone and in the presence of their cognate GTPase-activating proteins (GAPs) and guanine nucleotide exchange factors, are affected by the presence of the fluorescent mant moiety. Intrinsic hydrolysis of mantGTP by Ras homolog enriched in brain (Rheb) is ~10 times faster than that of GTP, whereas it is 3.4 times slower with RhoA. On the other hand, the mant tag inhibits TSC2GAP-catalyzed GTP hydrolysis by Rheb but promotes p120 RasGAP-catalyzed GTP hydrolysis by H-Ras. Guanine nucleotide exchange factor-catalyzed nucleotide exchange for both H-Ras and RhoA was inhibited by mant-substituted nucleotides, and the degree of inhibition depends highly on the GTPase and whether the assay measures association of mantGTP with, or dissociation of mantGDP from the GTPase. These results indicate that the mant moiety has significant and unpredictable effects on GTPase reaction kinetics and underscore the importance of validating its use in each assay.

The Ras superfamily of small GTPases plays vital roles in the integrated network of cellular signaling. They are "turned on" by binding to GTP and adopting a conformation that allows modulation of their downstream effectors. The proteins are then "turned off" by hydrolysis of the γ-phosphate of GTP and conversion to GDP (see Fig. 1*a*). The relative amounts of activated GTP-bound and inactive GDP-bound forms of GTPases are tightly regulated by GAPs,[5] which catalyze nucleotide hydrolysis, and GEFs, which promote nucleotide exchange. Mutation or unregulated expression of the small GTPase proteins or their respective GAPs and GEFs can deregulate the GTPase cycle and lead to diseases such as cancer, neurodegeneration, and mental disabilities (1).

Although several methods for monitoring GTP hydrolysis and nucleotide exchange of small GTPase proteins have been developed (1–4), the assay most widely used to monitor kinetics employs the fluorescently labeled guanosine nucleotide analogs mantGTP/mantGDP, which are sensitive to the hydrophobic environment of proteins (see Fig. 1*b*). Because of high sensitivity and selectivity, mantGTP and mantGDP have been widely used in the field (5–7); however, the use of these nucleotide analogs is justified only if they report reaction kinetics and thermodynamics that are consistent with the natural ligands GTP and GDP. Previously, some inconsistencies between native GTP and mantGTP were observed in nucleotide hydrolysis assays of Ras and RhoA with their cognate GAPs (8, 9). However, these fluorescent probes have never been fully assessed due to the lack of appropriate methodology.

Recently we developed an NMR-based real-time assay to monitor the rate of GTP hydrolysis of Ras homolog enriched in brain (Rheb), enabling us to monitor GTPase reactions using native GTP and GDP (supplemental Fig. S2*b*) (10). We have demonstrated that the real-time NMR methodology can be successfully used to assay nucleotide exchange in RhoA (11). This methodology requires no chemical modification of the protein or the nucleotide, which can perturb the native structure of the protein (supplemental Fig. S1), and has the ability to sense subtle changes in the rate of catalysis in real-time fashion. In this study, we employed the NMR methodology to examine how the fluorescent adduct on mantGTP and mantGDP affects the kinetics of nucleotide hydrolysis and exchange of three small GTPases (H-Ras, Rheb, and RhoA) alone and in the presence of their GAPs or GEFs.

EXPERIMENTAL PROCEDURES

Protein Preparation—Murine Rheb (residues 1–169), human H-Ras (residues 1–171), and murine RhoA (residues 1–181) were prepared as described in the supplemental material

* This work was supported by grants from the Cancer Research Society (Canada) and a United States Department of Defense Tuberous Sclerosis Complex Research Program Award (to V. S.).
[S] The on-line version of this article (available at http://www.jbc.org) contains supplemental Equations 1–6, Figs. S1–S5, and Tables S1 and S2.
[1] Supported by a postdoctoral fellowship from the Canadian Institutes of Health Research.
[2] Holds an Early Researcher Award from the Government of Ontario.
[3] Hold Canada Research Chairs.
[4] To whom correspondence should be addressed. Tel.: 416-581-7550; Fax: 416-581-7564; E-mail: mikura@uhnres.utoronto.ca.

[5] The abbreviations used are: GAP, GTPase-activating protein; GEF, guanine nucleotide exchange factor; mant, 2′(3′)-*O*-(*N*-methylanthraniloyl); mantGTP, 2′(3′)-*O*-(*N*-methylanthraniloyl)-GTP; mantGDP, 2′(3′)-*O*-(*N*-methylanthraniloyl)-GDP; DH-PH, Dbl homology-pleckstrin homology; GTPγS, guanosine 5′-3-*O*-(thio)triphosphate; ^{1}H-^{15}N HSQC, heteronuclear single quantum coherence; Rheb, Ras homolog enriched in brain; SOS, Son of Sevenless; dGppNHp, 2′-deoxyguanosine-5′-(β,γ-imido)-triphosphate.

Downloaded from www.jbc.org at TORONTO WESTERN HOSPITAL, on February 16, 2010

Supplemental Material can be found at:
http://www.jbc.org/content/suppl/2009/12/14/C109.064766.DC1.html

according to previous protocols (10, 12, 13). Tuberous sclerosis 2 (TSC2) GAP domain (residues 1525–1742: hereafter termed TSC2GAP) and the DH-PH fragment of PDZ-RhoGEF (residues 713–1081: hereafter termed DH-PH^{PRG}) were prepared using pGEX2T and pGEX4T1 vectors, respectively (10, 13). Catalytic domain constructs of the Son of Sevenless (SOS, Cdc25 residues 566–1049: hereafter referred to as Cdc25^{SOS}) and the GTPase-activating domain of human GTPase-activating protein p120GAP (residues 715–1047: hereafter referred to as RasGAP) were prepared as His-tagged proteins from the pET15b vector. All proteins were cleaved from their tags via thrombin.

NMR-based GTPase, GAP, and GEF Assays—H-Ras and Rheb were loaded with GTP or mantGTP by incubation with a 10-fold excess of nucleotide in the presence of 10 mM EDTA. RhoA was loaded with GTP or mantGTP in the presence of 0.5 M urea and 10 mM EDTA. A heteronuclear single quantum coherence (^{1}H-^{15}N HSQC) spectrum was collected to confirm full nucleotide loading, and the mixture was then passed through a desalting column (PD MidiTrap^{TM} G-25 (GE healthcare)) equilibrated with NMR buffer to produce a 1:1 complex of GTPase and the nucleotide.

All NMR experiments were run on a Bruker AVANCE II 800-MHz spectrometer equipped with a 5-mm TCI CryoProbe. Sensitivity-enhanced ^{1}H-^{15}N HSQCs with two scans (5 min) were run in succession to monitor the intrinsic GTP hydrolysis activity of GTPases (0.1–0.3 mM) at 20 °C. The spectra were processed with NMRPipe (14), and the peak heights were analyzed with Sparky (15) via Gaussian line fitting. Residues from switches I and II, P-loop, β3 and β4, and the α3 helix that exhibit distinct well resolved peaks in each nucleotide-bound state were used as reporters of the reaction rates for each of the three GTPases, as described previously for Rheb (10).

For the intrinsic nucleotide hydrolysis, the fraction of GTPase protein in the GDP-bound state was calculated for each reporter residue using supplemental Equation 1 for Ras and Rheb relying on both GDP and GTP peaks. In the case of RhoA, the active state exhibited broadened and split peaks that complicate peak integration; hence we monitored (see supplemental Equation 2) the appearance of GDP peaks. Data fitting was done using PRISM (GraphPad software).

To assay GAP-mediated nucleotide hydrolysis, RasGAP or TSC2GAP was added to GTP-loaded H-Ras or Rheb at a GAP-to-GTPase molar ratio of 1:2,500 or 1:2.2, respectively. The hydrolysis rate was determined by fitting the data to supplemental Equation 1.

For GEF assays, DH-PH^{PRG} or Cdc25^{SOS} was added at a molar ratio of 1:30,000 GEF to RhoA or Ras in the presence of a 10-fold molar excess of GTP or mantGTP. All the experiments were performed in duplicate with 0.1 mM GTPase. The observed rates of nucleotide exchange assays performed with hydrolyzable nucleotides are affected by intrinsic hydrolysis. Thus, the observed data were fitted to equations that consider both exchange and hydrolysis (see supplemental material, Equations 4 and 6) to extract the true exchange rate. Using this rate, an exponential decay curve was generated to approximate nucleotide exchange in the absence of hydrolysis.

RESULTS

The Effect of mant on the Intrinsic Rate of Nucleotide Hydrolysis—mant-substituted nucleotides have been used extensively to investigate many aspects of G-protein signaling, including the kinetics and mechanisms of RasGAP-mediated GTP hydrolysis (9, 16–18) and Cdc25^{SOS}-mediated nucleotide exchange (6, 7). We first used NMR methodology to examine whether the addition of the mant moiety alters the intrinsic hydrolysis rate of the GTPase domain of H-Ras (1–171) (Fig. 1*c*) and found that it had little effect (supplemental Table S1), consistent with previous reports (19).

Next, we analyzed GTP hydrolysis by Rheb, which shares ~33% sequence identity with H-Ras. Surprisingly, the hydrolysis rate of mantGTP by Rheb (3.2×10^{-3} min^{-1}) was >10 times faster than that of native GTP when both reactions were monitored by NMR (Fig. 1*c*). The rate constant obtained with mantGTP by NMR was identical to the value obtained using fluorescence spectroscopy (Fig. 1*c* and supplemental Fig. S2*a*), demonstrating that the results are independent of the detection method. Using mantGTP to compare the activity of different GTPases, the intrinsic GTPase activity of Rheb would appear approximately two times lower than that of H-Ras, whereas it is actually ~32 times lower with native GTP, demonstrating that reliance on mantGTP would overlook this biologically important difference.

As a third case, the effect of the mant substitution on the GTPase activity of RhoA, which shares ~31% sequence identity with H-Ras and Rheb, was investigated and found to be opposite to that observed with Rheb (Fig. 1*c*). The half-life of mantGTP bound to RhoA was ~155 min, 3.5-fold longer than that of native GTP (~45 min) (supplemental Table S1). Taken together, the results show that mant-substituted nucleotides can substantially alter the kinetics of nucleotide hydrolysis by small GTPases in a manner that could not have been predicted *a priori*.

The Effect of mant on the Rate of GAP-catalyzed Nucleotide Hydrolysis—Having established that mant can have a substantial effect on intrinsic GTPase reaction rates, we investigated the effect of mantGTP on GAP-accelerated GTPase reactions. First, we used the GAP domain of the human p120-RasGAP. GTP was hydrolyzed with a rate of 2.6×10^{-2} min^{-1} by H-Ras in the presence of a 1:2,500 molar ratio of RasGAP, whereas mantGTP was turned over approximately five times faster (Fig. 2*a* and supplemental Table S1). Indeed, Moore *et al.* (9) previously noted that in the presence of RasGAP, p21$^{N\text{-}Ras}$ hydrolyzes mantGTP more rapidly than native GTP, although the cleavage of the two nucleotides was not monitored by the same method.

We then examined how mantGTP might affect GAP-mediated GTP hydrolysis of a second, unrelated GAP with a distinct mechanism of action by studying Rheb and its well characterized GAP, TSC2GAP (10). At a TSC2GAP-to-Rheb ratio of 1:2.2, GTP was hydrolyzed at a rate of 1.9×10^{-2} min^{-1}, whereas mantGTP was hydrolyzed ~2.5-fold more slowly (Fig. 2*b* and supplemental Table S1). Comparing Rheb's intrinsic rate of mantGTP hydrolysis to the GAP-catalyzed rate, TSC2GAP only produced a 2-fold enhancement (supplemental Table S1). This contrasts sharply

Downloaded from www.jbc.org at TORONTO WESTERN HOSPITAL, on February 16, 2010

Supplemental Material can be found at:
http://www.jbc.org/content/suppl/2009/12/14/C109.064766.DC1.html

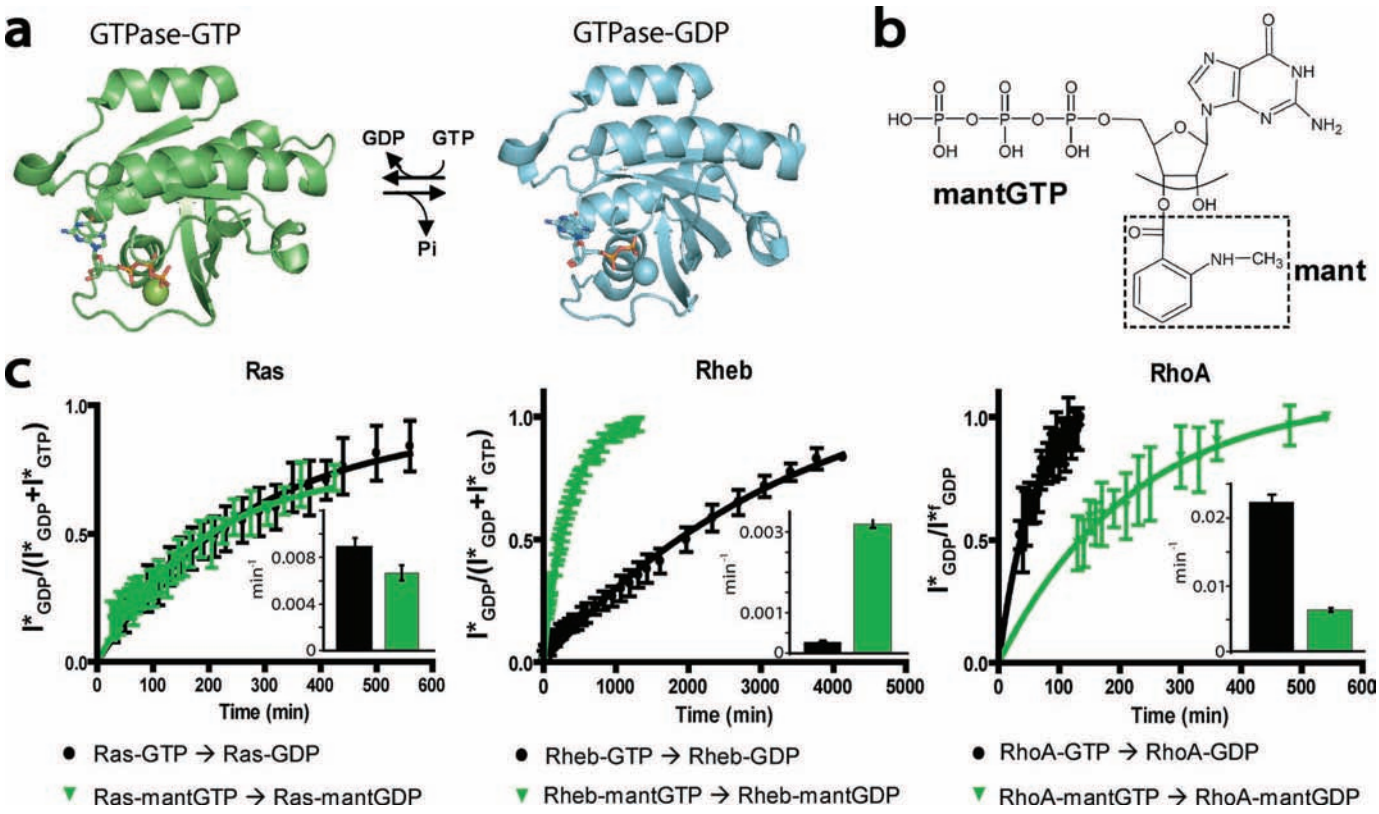

FIGURE 1. **Effect of mant-substituted GTP on the intrinsic nucleotide hydrolysis of Ras, Rheb, and RhoA.** *a*, nucleotide-dependent conformational changes in GTPases. Nucleotide hydrolysis and exchange are correlated with conformational changes that are readily probed in two-dimensional ^{1}H-^{15}N HSQC spectra (Protein Data Bank (PDB): 1XTS (29) *green*; 1XTQ (29) *cyan*). *b*, the chemical structure of mantGTP (ChemSketch (30)) is shown with the mant moiety at the 3′ position of the ribose ring. In solution, this moiety exhibits slow chemical exchange between the 2′ and 3′ positions of the ribose ring, producing an equilibrium ratio of 4:6 (31). *c*, the time course of intrinsic GTP (*black*) and mantGTP (*green*) hydrolysis by H-Ras, Rheb, and RhoA probed via real-time solution NMR spectroscopy. All the proteins were fully loaded with GTP or mantGTP before the start of the assay, as assessed by ^{1}H-^{15}N HSQC. The rates are displayed with a histogram for each curve in inserted *panel c*. See supplemental material for descriptions of the equations.

with the ~50-fold stimulation of Rheb GTPase activity by TSC2GAP when native GTP is used in the assay. Hence, exclusive use of mantGTP would lead to a gross underestimation of the GAP activity of TSC2 toward Rheb, underscoring the utility of the NMR-based methodology.

The Effect of mant on the GEF-mediated Nucleotide Exchange—We examined how mant-substituted nucleotides affect the DH-PH^{PRG}-mediated nucleotide exchange of RhoA (Fig. 3*a*) using a procedure described elsewhere (11). In the NMR GEF assay with hydrolyzable nucleotides, the readout (*i.e.* GDP- and GTP-specific protein cross-peaks) is determined by both exchange and intrinsic nucleotide hydrolysis. This is evident in the case of Ras and RhoA (Fig. 3), which do not become 100% saturated with GTP or mantGTP. Hence, the observed data were fit to an equation that considers exchange and hydrolysis (see supplemental material) to derive the true exchange rate. We have shown that this derived rate agrees well with the rate determined for the non-hydrolyzable GTPγS (11). In an assay of nucleotide association with RhoA, mantGTP exhibits a 30% lower exchange rate (4.9×10^{-2} min^{-1}) when compared with native GTP (7.0×10^{-2} min^{-1}) (supplemental Table S2). In the literature, both the incorporation (13, 20, 21) and the dissociation (22, 23) of the mant-substituted nucleotide have been employed to study the function of RhoA and its interaction with GEFs. Hence, we also performed the dissociation assay, initially loading RhoA with GDP or mantGDP and monitoring exchange to GTP. In this reaction, the rate of DH-PH^{PRG}-mediated nucleotide dissociation was approximately six times slower for mantGDP than for GDP (supplemental Fig. S3, *a* and *c*).

Previous studies have used mantGDP extensively to probe the Son of Sevenless (Cdc25^{SOS})-catalyzed nucleotide exchange of Ras GTPase. Generally, Ras is preloaded with mantGDP, and the decay in fluorescent intensity is monitored as this fluorescent nucleotide is displaced by unlabeled GTP (6, 7, 24–27). Here, using an NMR-based protocol similar to that described for RhoA, we show (Fig. 3*b* and supplemental Table S2) that the rate of Cdc25^{SOS}-catalyzed mantGDP dissociation (7.2×10^{-3} min^{-1}) is ~30% slower when compared with that of native GDP. GEF assays using association of mant-tagged nucleotide with Ras have also been reported (28); thus, we used NMR to compare the Cdc25^{SOS}-catalyzed association of mantGTP and GTP. We found that the rate of association of mantGTP with H-Ras is ~3-fold slower than that of GTP (supplemental Fig. S3, *b* and *d*).

DISCUSSION

Fluorescently labeled guanosine nucleotides have been used extensively to study nucleotide hydrolysis and exchange of GTPases. However, covalent modification of the nucleotide with a bulky fluorophore raises concerns about how this reporter moiety may perturb enzymatic activity. The NMR

Downloaded from www.jbc.org at TORONTO WESTERN HOSPITAL, on February 16, 2010

Supplemental Material can be found at:
http://www.jbc.org/content/suppl/2009/12/14/C109.064766.DC1.html

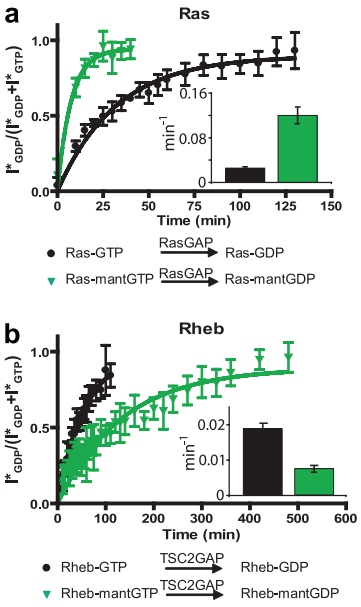

FIGURE 2. **Effects of mant-substituted GTP on GAP-mediated nucleotide hydrolysis by H-Ras and Rheb.** *a*, time course of RasGAP-mediated nucleotide hydrolysis of H-Ras with GTP (*black*) and mantGTP (*green*). A molar ratio of 1:2,500 RasGAP to H-Ras was used. *b*, time course of TSC2GAP-mediated hydrolysis of GTP (*black*) and mantGTP (*green*) bound to Rheb. A molar ratio of 1:2.2 TSC2GAP to Rheb was used for both assays. Rates extracted from each curve are displayed with an inserted histogram. Each experiment was performed in duplicate, and each curve represents a single representative experiment.

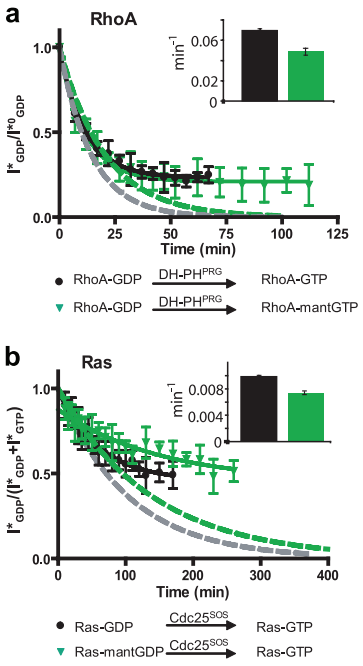

FIGURE 3. **Effects of mant-substituted nucleotides on GEF-mediated nucleotide exchange for H-Ras and RhoA.** *a*, time course of DH-PH^{PRG}-mediated nucleotide exchange of RhoA-GDP to GTP (*black*) and mantGTP (*green*). A molar ratio of 1:30,000 RhoA to DH-PH^{PRG} was used for both assays. *b*, time course of CDC25^{SOS}-mediated nucleotide exchange of H-Ras-GDP (*black*) and H-Ras-mantGDP (*green*) to GTP with 1:30,000 H-Ras to CDC25^{SOS} molar ratio. Observed data (*continuous lines*) were fitted to an equation that considers both exchange and hydrolysis to extract the true exchange rate k_{ex} in each experiment supplemental material). Using this rate, exponential decay curves (*dashed lines*) were generated to approximate nucleotide exchange in the absence of hydrolysis. The corrected rates are displayed with an inserted histogram for each curve. Each experiment was performed in duplicate, and each curve represents a single representative experiment.

methodology recently developed by our group (10) does not require any chemical modification of GTP or GDP because it makes direct observation of protein resonances that depend on nucleotide-induced changes in the chemical environment of protein (supplemental Fig. S2*b*). In this study, we employed this NMR method to compare native *versus* mant-labeled nucleotides in the kinetics of intrinsic GTPase reactions, GAP-mediated nucleotide hydrolysis, and GEF-mediated nucleotide exchange reactions of three small GTPases, H-Ras, Rheb, and RhoA. Our results clearly demonstrate that mant-labeled nucleotides had substantial effects on the kinetics of these reactions and that these effects were remarkably different and unpredictable with each GTPase, GAP, and GEF.

Intrinsic Hydrolysis of GTP and mantGTP—H-Ras exhibited a small decrease in the intrinsic hydrolysis rate of mantGTP *versus* native GTP; however, Rheb and RhoA were affected more drastically by this fluorescent tag. Remarkably, mant had opposite effects on Rheb and RhoA; Rheb hydrolyzed mantGTP ~10-fold faster than native GTP, whereas RhoA hydrolyzed this analog 3-fold more slowly than GTP. Thus, the effects of mant are specific to the structure and catalytic mechanism of each GTPase rather than the inherent lability of the nucleotide. With all three GTPases, the mant adduct perturbed proximal residues in the P-loop, switch I, and G-5 box but also induced long range perturbations in several regions including switch II (supplemental Fig. S4). The catalytic Gln of RhoA is found in switch II; thus, distortion of the structure of this loop could inhibit the hydrolysis of mantGTP. Interestingly, the analogous Gln in Rheb is in an orientation that does not contribute to catalysis (10, 29). To understand the rapid hydrolysis of mantGTP by Rheb, we asked whether the mant-induced perturbation of switch II might favor a catalytically competent conformation of Gln-64. However the Q64L mutation had no effect on hydrolysis of mantGTP, indicating that this reaction occurs through a more complex mechanism (supplemental Fig. S5).

GAP-catalyzed GTP Hydrolysis by H-Ras and Rheb—p120-RasGAP-catalyzed hydrolysis of mantGTP by H-Ras was ~5-fold faster than that of native GTP, whereas TSC2GAP-mediated hydrolysis of mantGTP by Rheb was slower by a factor of ~2.5 relative to unmodified GTP. Considering the rapid intrinsic GTPase activity of Rheb toward mantGTP, it is apparent that TSC2GAP activity is severely inhibited by mant. These results demonstrate the unpredictable effects of mant-tagged nucleotides on intrinsic and GAP-mediated GTPase activities and highlight the utility of the NMR approach.

Previous studies using a phosphate release assay showed that the K_m of p120 RasGAP-mediated hydrolysis of p21 N-Ras-mantGTP is lower than that of the p21 N-Ras-GTP complex (9). This result suggests that mant may increase the affinity of the H-Ras-nucleotide complex for RasGAP, thus increasing the rate of nucleotide hydrolysis. Conversely, we propose that for Rheb, the mant moiety probably hinders docking of the TSC2GAP domain to Rheb. Note that TSC2 and p120 RasGAP are not homologous, have different folds, and function through distinct catalytic mechanisms. Further structural insights are required to address the mechanistic basis for the "mant effect" on GAP-mediated nucleotide hydrolysis for both H-Ras and Rheb.

Downloaded from www.jbc.org at TORONTO WESTERN HOSPITAL, on February 16, 2010

Supplemental Material can be found at:
http://www.jbc.org/content/suppl/2009/12/14/C109.064766.DC1.html

GEF-accelerated Nucleotide Exchange of H-Ras and RhoA—Using the aforementioned NMR-based approach (11), we performed GEF assays to measure both association and dissociation of mant-tagged nucleotides as fluorescence-based experiments have been reported both ways in the literature (6, 7, 13, 20–23, 24–28). Comparing dissociation, $Cdc25^{SOS}$-mediated nucleotide exchange was 30% slower when starting with mantGDP-bound H-Ras (mantGDP-to-GTP) than with GDP-bound H-Ras (GDP-to-GTP). Measuring association under the same conditions, the GDP-to-mantGTP exchange was approximately three times slower than the GDP-to-GTP exchange. Similarly, $DH\text{-}PH^{PRG}$-mediated nucleotide exchange was 30% slower for the GDP-to-mantGTP than the GDP-to-GTP exchange in the association assay and ~6-fold slower for the mantGDP-to-GTP than the GDP-to-GTP exchange in the dissociation assay. In the crystal structure of H-Ras-mant dGppNHp (12), mant is near residue Tyr-31 in switch I, which would introduce steric clashes at the primary contact point between the GTPase and $Cdc25^{SOS}$ and could interfere with nucleotide exchange. Assuming that the mant moiety of the nucleotide is similarly positioned on the switch I region of RhoA, it would also hinder $DH\text{-}PH^{PRG}$ binding to RhoA (13). Furthermore, mant-induced structural perturbations of the GEF binding sites in the GTPase switch regions may inhibit interactions with GEFs. The exchange kinetics reported by mant are more reliable when the dissociation assay is used for the Ras-$CDC25^{SOS}$ system and when the association assay is used for the RhoA-$DH\text{-}PH^{PRG}$ system. Note that these are the conventional fluorescence methods for each protein; nevertheless, the less accurate alternative approaches are still in use. Finally, the reduced sensitivity of mantGDP-bound GTPases to the action of GEFs suggests an avenue for design of GTPase inhibitors.

In conclusion, we have demonstrated that mant-labeled nucleotides can alter the intrinsic GTPase activity of Rheb and RhoA, the GAP-catalyzed GTP hydrolysis of H-Ras-RasGAP and Rheb-TSC2GAP, as well as the $DH\text{-}PH^{PRG}$- and $CDC25^{SOS}$-mediated nucleotide exchange of RhoA and H-Ras, respectively. These results reveal that the fluorescent probes could yield biochemically inaccurate data and potentially lead to misleading conclusions. The significant and unpredictable effects of the mant tag clearly indicate that mant-tagged nucleotides should be used with caution and should be validated for each GTPase system studied. At the same time, these findings provide clues as to how one could inhibit or activate specific signaling pathways using small organic molecules, which may mimic the effects of the mant tag on small GTPases. This study also extends the utility and value of the NMR-based assays for both GTPase and GEF reactions for three small GTPases, suggesting that it will be broadly applicable to the GTPase superfamily.

Acknowledgment—800- and 600-MHz NMR spectrometers were funded by the Canada Foundation for Innovation.

REFERENCES

1. Ahmadian, M. R., Wiesmüller, L., Lautwein, A., Bischoff, F. R., and Wittinghofer, A. (1996) *J. Biol. Chem.* **271,** 16409–16415
2. Albert, S., and Gallwitz, D. (2000) *Biol. Chem.* **381,** 453–456
3. Futai, E., Hamamoto, S., Orci, L., and Schekman, R. (2004) *EMBO J.* **23,** 4146–4155
4. Zhang, B., and Zheng, Y. (1998) *Biochemistry* **37,** 5249–5257
5. Mou, T. C., Gille, A., Fancy, D. A., Seifert, R., and Sprang, S. R. (2005) *J. Biol. Chem.* **280,** 7253–7261
6. Gureasko, J., Galush, W. J., Boykevisch, S., Sondermann, H., Bar-Sagi, D., Groves, J. T., and Kuriyan, J. (2008) *Nat. Struct. Mol. Biol.* **15,** 452–461
7. Sondermann, H., Soisson, S. M., Boykevisch, S., Yang, S. S., Bar-Sagi, D., and Kuriyan, J. (2004) *Cell* **119,** 393–405
8. Eberth, A., Dvorsky, R., Becker, C. F., Beste, A., Goody, R. S., and Ahmadian, M. R. (2005) *Biol. Chem.* **386,** 1105–1114
9. Moore, K. J., Webb, M. R., and Eccleston, J. F. (1993) *Biochemistry* **32,** 7451–7459
10. Marshall, C. B., Ho, J., Buerger, C., Plevin, M. J., Li, G. Y., Li, Z., Ikura, M., and Stambolic, V. (2009) *Sci. Signal.* **2,** ra3
11. Gasmi-Seabrook, G. M. C., Marshall, C. B., Cheung, M., Kim, B., Wang, F., Jang, Y. J., Mak, T. W., Stambolic, V., and Ikura, M. (2010) *J. Biol. Chem.* **285,** 5137–5145
12. Scheidig, A. J., Franken, S. M., Corrie, J. E., Reid, G. P., Wittinghofer, A., Pai, E. F., and Goody, R. S. (1995) *J. Mol. Biol.* **253,** 132–150
13. Derewenda, U., Oleksy, A., Stevenson, A. S., Korczynska, J., Dauter, Z., Somlyo, A. P., Otlewski, J., Somlyo, A. V., and Derewenda, Z. S. (2004) *Structure* **12,** 1955–1965
14. Delaglio, F., Grzesiek, S., Vuister, G. W., Zhu, G., Pfeifer, J., and Bax, A. (1995) *J. Biomol. NMR* **6,** 277–293
15. Goddard, T. D., and Kneller, D. G. *SPARKY* 3, University of California, San Francisco, CA
16. Phillips, R. A., Hunter, J. L., Eccleston, J. F., and Webb, M. R. (2003) *Biochemistry* **42,** 3956–3965
17. Ahmadian, M. R., Wittinghofer, A., and Herrmann, C. (2002) *Methods Mol. Biol.* **189,** 45–63
18. Ahmadian, M. R., Hoffmann, U., Goody, R. S., and Wittinghofer, A. (1997) *Biochemistry* **36,** 4535–4541
19. Remmers, A. E., Posner, R., and Neubig, R. R. (1994) *J. Biol. Chem.* **269,** 13771–13778
20. Hutchinson, J. P., and Eccleston, J. F. (2000) *Biochemistry* **39,** 11348–11359
21. Oleksy, A., Barton, H., Devedjiev, Y., Purdy, M., Derewenda, U., Otlewski, J., and Derewenda, Z. S. (2004) *Acta Crystallogr. D. Biol. Crystallogr.* **60,** 740–742
22. Tan, Y. C., Wu, H., Wang, W. N., Zheng, Y., and Wang, Z. X. (2002) *Anal. Biochem.* **310,** 156–162
23. Hemsath, L., and Ahmadian, M. R. (2005) *Methods* **37,** 173–182
24. Ford, B., Hornak, V., Kleinman, H., and Nassar, N. (2006) *Structure* **14,** 427–436
25. Margarit, S. M., Sondermann, H., Hall, B. E., Nagar, B., Hoelz, A., Pirruccello, M., Bar-Sagi, D., and Kuriyan, J. (2003) *Cell* **112,** 685–695
26. Freedman, T. S., Sondermann, H., Friedland, G. D., Kortemme, T., Bar-Sagi, D., Marqusee, S., and Kuriyan, J. (2006) *Proc. Natl. Acad. Sci. U.S.A.* **103,** 16692–16697
27. Ford, B., Skowronek, K., Boykevisch, S., Bar-Sagi, D., and Nassar, N. (2005) *J. Biol. Chem.* **280,** 25697–25705
28. Sacco, E., Metalli, D., Busti, S., Fantinato, S., D'Urzo, A., Mapelli, V., Alberghina, L., and Vanoni, M. (2006) *FEBS Lett.* **580,** 6322–6328
29. Yu, Y., Li, S., Xu, X., Li, Y., Guan, K., Arnold, E., and Ding, J. (2005) *J. Biol. Chem.* **280,** 17093–17100
30. Spessard, G. O. (1998) *J. Chem. Inf. Comput. Sci.* **38,** 1250–1253
31. Neal, S. E., Eccleston, J. F., and Webb, M. R. (1990) *Proc. Natl. Acad. Sci. U.S.A.* **87,** 3562–3565

Downloaded from www.jbc.org at TORONTO WESTERN HOSPITAL, on February 16, 2010

Supplemental Material can be found at:
http://www.jbc.org/content/suppl/2009/12/17/M109.064691.DC1.html

THE JOURNAL OF BIOLOGICAL CHEMISTRY VOL. 285, NO. 8, pp. 5137–5145, February 19, 2010
© 2010 by The American Society for Biochemistry and Molecular Biology, Inc. Printed in the U.S.A.

Real-time NMR Study of Guanine Nucleotide Exchange and Activation of RhoA by PDZ-RhoGEF*[S]

Received for publication, September 10, 2009, and in revised form, November 20, 2009 Published, JBC Papers in Press, December 17, 2009, DOI 10.1074/jbc.M109.064691

Geneviève M. C. Gasmi-Seabrook[‡§], Christopher B. Marshall[‡§], Melissa Cheung[‡§], Bryan Kim[‡§], Feng Wang[‡§], Ying Ju Jang[§¶], Tak W. Mak[§¶], Vuk Stambolic[‡§1], and Mitsuhiko Ikura[‡§2]

From the [‡]Division of Signaling Biology and [¶]The Campbell Family Institute, Ontario Cancer Institute, University Health Network, Toronto, Ontario M5G 1L7 and the [§]Department of Medical Biophysics, University of Toronto, Toronto, Ontario M5G 2M9, Canada

Small guanosine triphosphatases (GTPases) become activated when GDP is replaced by GTP at the highly conserved nucleotide binding site. This process is intrinsically very slow in most GTPases but is significantly accelerated by guanine nucleotide exchange factors (GEFs). Nucleotide exchange in small GTPases has been widely studied using spectroscopy with fluorescently tagged nucleotides. However, this method suffers from effects of the bulky fluorescent moiety covalently attached to the nucleotide. Here, we have used a newly developed real-time NMR-based assay to monitor small GTPase RhoA nucleotide exchange by probing the RhoA conformation. We compared RhoA nucleotide exchange from GDP to GTP and GTP analogues in the absence and presence of the catalytic DH-PH domain of PDZ-RhoGEF (DH-PH^{PRG}). Using the non-hydrolyzable analogue guanosine-5′-*O*-(3-thiotriphosphate), which we found to be a reliable mimic of GTP, we obtained an intrinsic nucleotide exchange rate of 5.5×10^{-4} min^{-1}. This reaction is markedly accelerated to 1179×10^{-4} min^{-1} in the presence of DH-PH^{PRG} at a ratio of 1:8,000 relative to RhoA. Mutagenesis studies confirmed the importance of Arg-868 near a conserved region (CR3) of the Dbl homology (DH) domain and revealed that Glu-741 in CR1 is critical for full activity of DH-PH^{PRG}, together suggesting that the catalytic mechanism of PDZ-RhoGEF is similar to Tiam1. Mutation of the single RhoA (E97A) residue that contacts the pleckstrin homology (PH) domain rendered the mutant 10-fold less sensitive to the activity of DH-PH^{PRG}. Interestingly, this mutation does not affect RhoA activation by leukemia-associated RhoGEF (LARG), indicating that the PH domains of these two homologous GEFs may play different roles.

The small GTPase[3] RhoA, a member of the Ras superfamily, plays a crucial role in cellular processes including proliferation, movement, cell shape, as well as cell-cell and cell-matrix interactions (1). RhoA acts as a molecular switch, cycling between the inactive GDP- and activated GTP-bound states (Fig. 1*A*). Akin to other small GTPases, RhoA contains a phosphate binding loop (P-loop) and two switch regions that undergo conformational changes upon nucleotide cycling and mediate interactions with effector proteins. Together these three regions interact with the nucleotide phosphate groups and a magnesium ion that is required for high affinity nucleotide binding (low nM to sub nM K_d). GTPase-activating proteins catalyze nucleotide hydrolysis, thus inactivating GTPases, whereas guanine nucleotide exchange factors (GEFs) activate GTPases by stimulating nucleotide exchange (2). PDZ-RhoGEF, like its homologues LARG and p115-RhoGEF, is specific to RhoA and is activated by the $G\alpha_{12/13}$ subunit of G-protein coupled receptors via its regulator of G-protein signaling domain. Interestingly, PDZ-RhoGEF single nucleotide polymorphisms have been associated with type II diabetes (3) and lung cancer (4).

RhoGEFs are multidomain proteins (5), most of which contain a conserved catalytic Dbl homology (DH) domain with an associated pleckstrin homology (PH) domain (6, 7). Interactions between the DH domains and Rho GTPases induce structural changes of the nucleotide binding pocket and stabilize the nucleotide-free form of Rho (6). Although the DH domain is required for GEF activity, the PH domain plays multiple roles including stabilizing the DH domain, directing its subcellular localization, and regulating GEF activity (6, 7). DH domains are comprised of a helix bundle in which three highly conserved regions (CR1, CR2, and CR3) constitute the core domain. The DH domain interacts extensively, through CR1 and CR3, with the switch regions of the cognate GTPase as illustrated in the crystal structure of PDZ-RhoGEF (DH-PH^{PRG}) in complex with RhoA (1XCG) (7). A highly conserved glutamate in CR1 and a conserved basic residue near CR3 (Fig. 2) have been implicated in the formation of the GEF-GTPase complex and in the nucleotide exchange catalysis in many RhoGEFs (6–8). Although mutations of the CR1 and CR3 region were found to affect the GEF activity of Tiam1 and Trio (6, 8, 9), the importance of the CR1 for PDZ-RhoGEF activity has not been investigated.

* This work was supported by a grant from the Cancer Research Society (Canada).

The backbone assignments reported in this paper have been submitted to the Biological Magnetic Resonance Data Bank under entries 16668 and 16669.

[S] The on-line version of this article (available at http://www.jbc.org) contains supplemental text and Figs. S1–S7.

[1] Holds an Early Researcher Award from the Government of Ontario.

[2] Holds a Canada Research Chair. To whom correspondence should be addressed: MaRS Toronto Medical Discovery Tower, Rm. 4-804, 101 College St., Toronto, ON M5G 1L7, Canada. Tel.: 416-581-7550; Fax: 416-581-7564; E-mail: mikura@uhnres.utoronto.ca.

[3] The abbreviations used are: GTPase, guanosine triphosphatase; GTPγS, guanosine-5′-*O*-(3-thiotriphosphate); GMPPNP, guanylyl imidodiphosphate; mant-GTP, *N*-methylanthraniloyl guanosine triphosphate; GEF, guanine nucleotide exchange factor; DH, Dbl homology; PH, pleckstrin homology; DH-PH^{PRG}, catalytic DH-PH domain of PDZ-RhoGEF; LARG, leukemia-associated RhoGEF; ^{1}H-^{15}N HSQC, ^{1}H-^{15}N heteronuclear single quantum coherence; TCEP, tris(2-carboxyethyl)phosphine.

Downloaded from www.jbc.org at TORONTO WESTERN HOSPITAL, on February 16, 2010

Supplemental Material can be found at:
http://www.jbc.org/content/suppl/2009/12/17/M109.064691.DC1.html

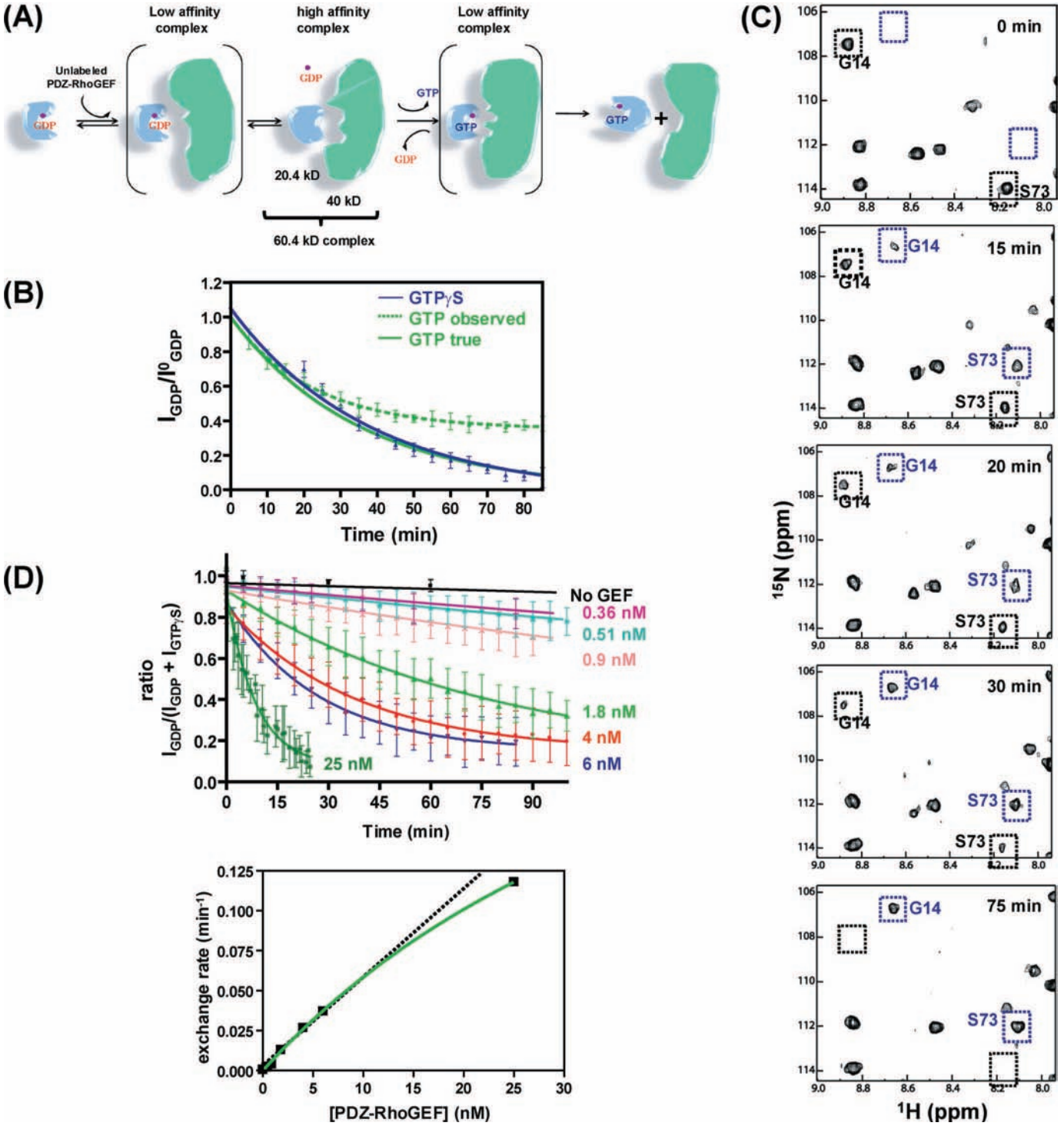

FIGURE 1. **RhoA nucleotide exchange in the presence of DH-PH^{PRG} monitored by NMR.** *A*, schematic of RhoA nucleotide exchange mediated by DH-PH^{PRG}. ^{15}N-labeled RhoA (*blue*, 20.4 kDa) with GDP and Mg^{2+} (*purple*) bound is in an inactive state. DH-PH^{PRG} (*green*, 43 kDa) interacts with residues in the RhoA switch regions, promoting the release of GDP. Subsequently, GTP binds RhoA, and the GEF is released to produce the activated form of RhoA. *B*, kinetics of RhoA-GDP nucleotide exchange to GTP (*green dashed line*) and GTPγS (*blue*) measured by the real-time NMR assay. A theoretical GTP exchange curve corrected for hydrolysis (see supplemental material) is also presented (*green solid line*) *Error bars* indicate S.D. for values reported by multiple peaks. *C*, snapshots of ^{1}H-^{15}N HSQC spectra during the 75-min time course of RhoA-GDP to GTPγS nucleotide exchange, in the presence of DH-PH^{PRG} (6 nM). *Black* and *blue boxes* indicate the positions of the RhoA-GDP and RhoA-GTPγS cross peaks, respectively, for Gly-14 and Ser-73. *D*, RhoA-GDP to GTPγS nucleotide exchange, with increasing concentration of DH-PH^{PRG}. The intrinsic nucleotide exchange rate is shown in *black*. Nucleotide exchange rates *k* (10^{-4} min^{-1}) are 5.5, 19, 24, 39, 130, 267, 371, and 1,179 for GEF concentrations of 0, 0.36, 0.51, 0.9, 1.8, 4, 6, 25 nM, respectively. *Lower panel*, the hyperbolic (*green curve*) dependence, on GEF concentration, of the nucleotide exchange rate is indicative of a two-step binding model.

The PH domain is comprised of seven antiparallel β-strands topped by a helix containing a partially conserved residue (Ser-1065 in PDZ-RhoGEF) that interacts with Glu-97 of RhoA (7). The DH domain alone is ~41-fold less active than the DH-PH domain of PDZ-RhoGEF (7), but it is also less stable; thus the importance of the RhoA PH domain interaction for GEF activity is not clear.

Downloaded from www.jbc.org at TORONTO WESTERN HOSPITAL, on February 16, 2010

Supplemental Material can be found at:
http://www.jbc.org/content/suppl/2009/12/17/M109.064691.DC1.html

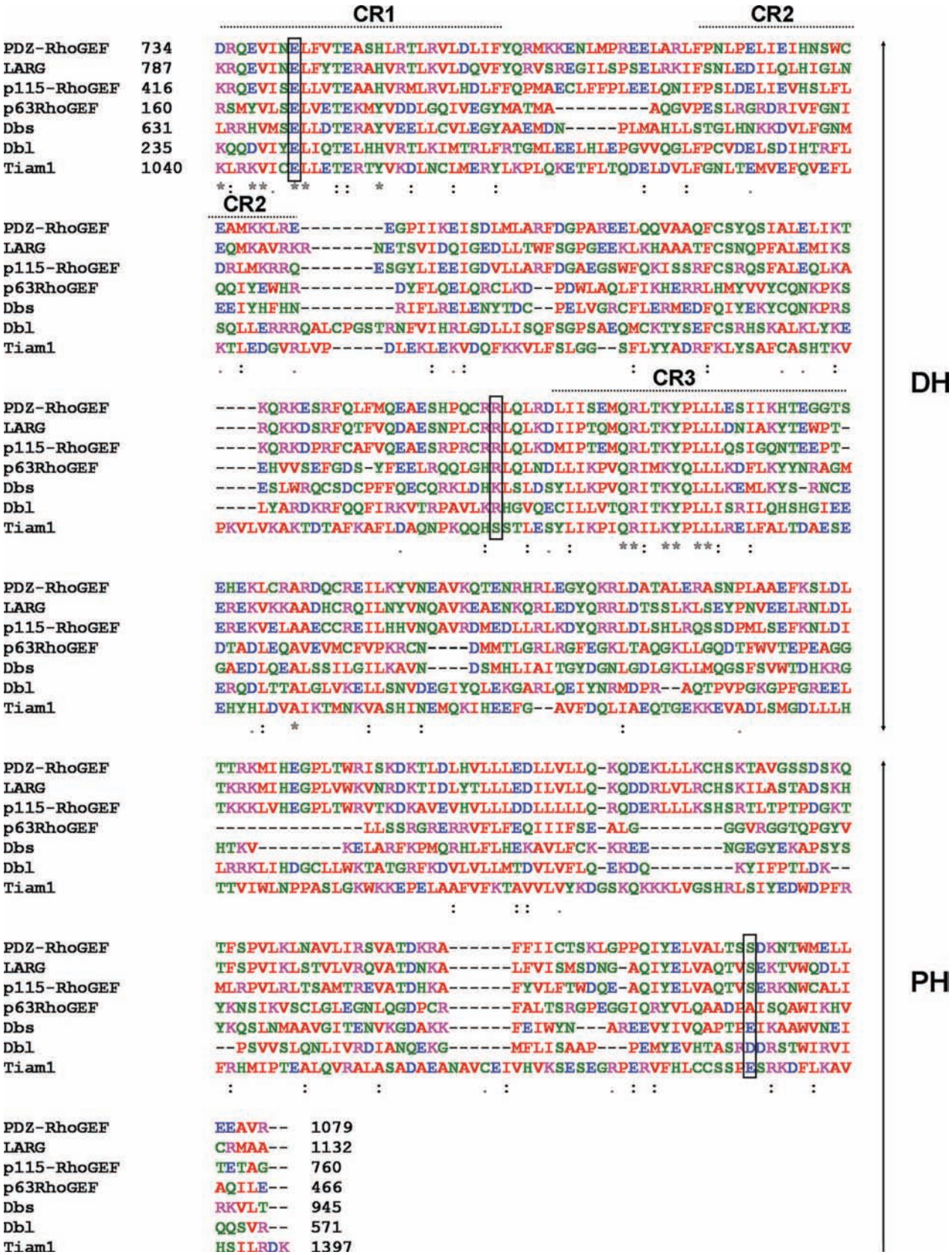

FIGURE 2. **Sequence alignment of DH-PH domains of human RhoGEFs.** PDZ-RhoGEF (O15085, residues 734–923), LARG (Q9NZN5, residues 787–977), p115-RhoGEF (Q92888, residues 416–605), Dbl-GEF (Q92974,, residues 235–432), p63-RhoGEF (Q86VW2, residues 160–336), Dbs-GEF (O15068, residues 631–811), and Tiam1 (Q13009, residues 1,040–1,234) were aligned using Clustal_W2. Hydrophobic, acidic, basic, and polar residues are indicated in *red*, *blue*, *magenta*, and *green*, respectively. The *stars* mark residues conserved throughout Rho guanine nucleotide exchange factors. *Colons* correspond to conserved substitutions and, *periods* correspond to semiconserved substitutions. Conserved residues examined in this study (Glu-741, Arg-868, and Ser-1065) are *boxed*. CR1, CR2, and CR3 are three highly conserved regions of the DH domain.

Downloaded from www.jbc.org at TORONTO WESTERN HOSPITAL, on February 16, 2010

Supplemental Material can be found at:
http://www.jbc.org/content/suppl/2009/12/17/M109.064691.DC1.html

We recently developed an NMR-based, real-time assay to measure the kinetics of GTP hydrolysis by the small GTPase Rheb by monitoring nucleotide-dependent changes in the NMR spectra of the GTPase protein (10). In this report, the NMR GTPase assay was extended to monitor intrinsic and PDZ-RhoGEF-mediated RhoA nucleotide exchange using native GDP and GTP as substrates. Our data show that PDZ-RhoGEF favors RhoA activation by catalyzing the exchange from GDP to GTP, severalfold more efficiently than the reverse reaction. Our mutagenesis studies demonstrate that Arg-868 near the CR3 and Glu-741 in the CR1 are critical for the full activity of PDZ-RhoGEF. We also found that RhoA Glu-97 is required for full activation by DH-PH^{PRG}, suggesting that the PH domain plays an important role in catalysis. While investigating PDZ-RhoGEF-mediated RhoA nucleotide exchange reactions using different nucleotides, we discovered that GTPγS better mimics GTP than the analogues mant-GTP or GMPPNP.

EXPERIMENTAL PROCEDURES

Protein Expression and Purification of RhoA and DH-PH^{PRG}—A construct encoding human RhoA residues 1–181 was cloned into pET28A using NdeI and EcoRI restriction endonucleases and expressed in *Escherichia coli* BL21(DE3) cells as a His$_6$-tagged protein The cells were grown in isotope-supplemented M9 media with 100 μg/ml kanamycin and induced at A_{600} = 0.8 with 0.25 mM isopropyl β-D-1-thiogalactopyranoside overnight at 15 °C. To prepare samples for resonance assignment, 2 g/liter [^{13}C]glucose and 1 g/liter [^{15}N]ammonium chloride were added to the media, whereas unlabeled glucose and [^{15}N]ammonium chloride were used to prepare samples for the nucleotide exchange assays. The cells were harvested by centrifugation, resuspended with lysis buffer (50 mM Tris, pH 8, 150 mM NaCl, 5 mM $MgCl_2$, 10% glycerol, 10 mM imidazole, 10 mM β-mercaptoethanol, 0.1% Nonidet P-40, 0.1 mM GDP, 1 mM phenylmethylsulfonyl fluoride), and sonicated, and the supernatant was stirred with nickel-nitrilotriacetic acid agarose (Qiagen) for 1 h at 4 °C. The resin was washed, and the protein was eluted with 50 mM Tris (pH = 8), 150 mM NaCl, 10% glycerol, 250 mM imidazole, 10 mM β-mercapto-ethanol, 5 mM $MgCl_2$. Thrombin was used to cleave the His tag during dialysis against 50 mM Tris (pH 8), 150 mM NaCl, 2% glycerol, 5 mM $MgCl_2$, 2 mM dithiothreitol, and 2 mM TCEP. Final purification of RhoA was achieved by gel filtration chromatography (Superdex S75 20/60, GE Healthcare) with 20 mM HEPES (pH 7.0), 100 mM NaCl, 5 mM $MgCl_2$, and 2 mM TCEP. A construct encoding the DH and PH domains of human PDZ-RhoGEF (DH-PH^{PRG}, residues 713–1,081) was subcloned into the vector PGEX 4T between the BamHI and EcoRI restriction endonuclease sites. DH-PH^{PRG} was expressed as a glutathione *S*-transferase fusion protein in *E. coli* BL21(DE3) Codon+ cells in Luria-Bertani broth supplemented with ampicillin and chloramphenicol (100 and 50 μg/ml, respectively) by induction with 0.25 mM isopropyl β-D-1-thiogalactopyranoside at 15 °C overnight. Following cell lysis by sonication, the fusion protein was enriched by binding to glutathione-Sepharose resin (GE Healthcare), eluted with 20 mM reduced glutathione, cleaved with thrombin overnight, and dialyzed against 10 mM Tris, pH 7.5, 150 mM NaCl, 2% glycerol, 2 mM dithiothreitol. Glutathione *S*-transferase was removed by an ion exchange HiTrap SP column using 20 mM Tris, pH 7.5, 1 mM dithiothreitol, and a 50–500 mM NaCl gradient. PDZ-RhoGEF DH-PH (713–1,081) domain was purified to homogeneity by gel filtration chromatography (Superdex 75 20/60) and concentrated in an Amicon 30,000 nominal molecular weight limit centrifugal concentrator. The mutants RhoA-E97A, DH-PH^{PRG}-E741A, DH-PH^{PRG}-E741D, and DH-PH^{PRG}-R868G were generated using QuikChange mutagenesis (Stratagene) according to the manufacturer's instructions.

Circular Dichroism—CD spectra were recorded for the wild-type and mutant forms of DH-PH^{PRG} in 20 mM HEPES buffer, pH 7, 100 mM NaCl, 5 mM $MgCl_2$, 2 mM TCEP using a cell with a 1-mm path length, at room temperature, on a Jasco J-815 CD spectrometer.

NMR Resonance Assignments—NMR experiments were performed at 20 °C on a 800-MHz Bruker AVANCE II spectrometer, equipped with a 5-mm TCI CryoProbe, and on a four-channel Varian Inova 600-MHz spectrometer equipped with *z* axis pulsed field gradient units and room temperature shielded triple resonance probes. NMR data were processed and analyzed using the NMRPipe (11) and NMRView programs (12). Chemical shift assignments were obtained using a ^{15}N, ^{13}C double-labeled sample of 0.3 mM RhoA-GDP or RhoA-GTPγS in 20 mM HEPES buffer, 100 mM NaCl, 5 mM $MgCl_2$, 2 mM TCEP, 10% D_2O, pH 7. Amide backbones ^{1}H, ^{15}N, CO, H_α, C_α, and C_β were assigned using two-dimensional ^{1}H-^{15}N heteronuclear single quantum coherence (HSQC) and the conventional three-dimensional triple-resonance experiments (13, 14), HNCACB, CBCA(CO)NH, HN(CA)CO, HNCO, HNHA, and three-dimensional ^{15}N-edited-nuclear Overhauser effect spectroscopy HSQC with a mixing time of 100 ms.

Nucleotide Exchange Assays—RhoA nucleotide exchange was monitored using NMR spectroscopy by acquiring successive ^{1}H-^{15}N HSQC spectra (two scans, 5-min acquisition time) at 20 °C over a period of time. DH-PH^{PRG} was added to ^{15}N-labeled GDP-bound RhoA (or ^{15}N-labeled GTPγS-bound RhoA) along with a 5-fold molar excess of nucleotide (GTP or analogue) at time 0. Nine assigned RhoA amides, with distinct chemical shifts in the GDP- and GTPγS-bound form, were used to evaluate the fraction of GDP-bound RhoA remaining in each spectrum. The data were fitted to a single phase exponential decay function to obtain the exchange rate k_{ex} for non-hydrolyzable analogues. For hydrolyzable nucleotides, k_{ex} was determined by fitting the data to an equation that considers both the nucleotide exchange and hydrolysis (see supplemental material for a more detailed methodology).

Concentration dependence of the GEF activity of DH-PH^{PRG} was assessed using 0.2 mM ^{15}N-labeled RhoA GDP-bound, 1 mM GTPγS, and unlabeled DH-PH^{PRG} at concentrations from 0.36 to 25 nM. DH-PH^{PRG} mutation studies were performed with 0.2 mM [^{15}N]-RhoA-GDP and 1.8 nM DH-PH^{PRG} (wild-type or mutants E741A, E741D, or R868G) and 1 mM GTPγS. Each of these mutants was determined to be well folded on the basis of circular dichroism spectra (supplemental Fig. S1). The nucleotide exchange assays of wild-type RhoA (0.2 mM) and

Downloaded from www.jbc.org at TORONTO WESTERN HOSPITAL, on February 16, 2010

Supplemental Material can be found at:
http://www.jbc.org/content/suppl/2009/12/17/M109.064691.DC1.html

the E97A mutant (0.2 mM) were compared using 4 nM DH-PH^{PRG} and a 5-fold molar excess of GTPγS.

A competition assay was carried out to assess the relative affinities of RhoA for different nucleotides. A series of ^{1}H-^{15}N HSQC spectra were recorded over 24 h following the addition of DH-PH^{PRG} (4 nM) and a mixture of GTP, GTPγS, GMPPNP, and mant-GTP (each 1 mM) to ^{15}N-labeled RhoA-GDP (0.2 mM). Binding of these nucleotides was assessed using the cross-peak of Gln-29, which exhibits distinct chemical shifts with each nucleotide.

RESULTS AND DISCUSSION

RhoA Nucleotide Exchange Stimulated with DH-PH^{PRG}—To explore the possibility of using the NMR assay for RhoA nucleotide exchange, we first sought to assign backbone resonances of RhoA. Using the standard triple-resonance approach, we were able to assign nearly 90% of the RhoA-GDP backbone amide ^{1}H and ^{15}N resonances (supplemental Fig. S2*a*), as well as the C_{α}, C_{β}, and CO resonances. A few residues in switch I, switch II, and the P-loop could not be assigned due to severe peak broadening. The secondary structure of RhoA-GDP predicted by the chemical shift index approach (15) is consistent with the crystal structure (16) (supplemental Fig. S3*a*). We also assigned 111 out of 132 amide resonances present in the ^{1}H-^{15}N HSQC of RhoA in the GTPγS-bound state (supplemental Fig. S2*b*). A significant number of amide cross peaks, particularly those in the P-loop and switch regions, were missing in the spectrum. Peak intensities for some of the broadened amides increased when the temperature was elevated from 20 to 40 °C (supplemental Fig. S4, *dash boxed insets*), indicative of intermediate chemical exchange on the NMR time scale. Similar phenomena were previously reported for Rheb-GMPPNP (10) and c-Ha-Ras (17). These results suggest that the nucleotide binding site of RhoA is in equilibrium between two or more conformational states when bound to GTPγS. Comparison of the ^{1}H-^{15}N HSQC spectra of RhoA-GDP and RhoA-GTPγS shows that amides located in the P-loop, the switch regions, and amides near the binding site display the largest chemical shift changes (supplemental Fig. S3*b*). Although rapid hydrolysis precluded independent assignment of the GTP-bound form, assignments for most peaks in the HSQC spectrum of RhoA-GTP could be transferred from that of RhoA-GTPγS, which is markedly similar (supplemental Fig. S5).

We used ^{1}H-^{15}N HSQC spectra to monitor RhoA intrinsic nucleotide exchange from GDP to GTP. When a 10-fold excess of GTP was added to ^{15}N-labeled GDP-loaded RhoA, the ^{1}H-^{15}N HSQC spectrum remained nearly identical to the spectrum of the GDP-loaded form for several days, indicating that intrinsic exchange is slow relative to intrinsic hydrolysis. With the addition of DH-PH^{PRG}, RhoA-GTP peaks appeared and RhoA-GDP peak intensities decreased, indicative of nucleotide exchange. With a GEF:RhoA ratio of 1:50,000 the observed nucleotide exchange reaction plateaus at $I_{GDP}/I^{0}_{GDP} \sim 0.4$ after 1 h (Fig. 1*B*, *dotted line*) due to GTP hydrolysis. A true k_{ex} rate of 286×10^{-4} min^{-1} was obtained by fitting the observed data to an equation (see supplemental Equation 2) that considers both exchange and hydrolysis. This true GTP k_{ex} value was used to plot an exponential decay curve representing the exchange component (Fig. 1*B*, *green curve*) and was compared with the exchange rate constants obtained with three analogues, GTPγS, GMPPNP, and mant-GTP. The results revealed that GTPγS exchanges with kinetics similar to GTP ($k_{ex} = 265.5 \times 10^{-4}$ min^{-1}, Fig. 1*B*, *blue line*), whereas GMPPNP and mant-GTP produced significantly slower rate constants (see "Effects of GTP Analogues on the Structure and Exchange Kinetics of RhoA"). Therefore GTPγS was substituted for GTP in the following nucleotide exchange assays, eliminating the GTP hydrolysis component.

To determine a GEF concentration range amenable to our nucleotide exchange assay, we performed a series of nucleotide exchange assays on [^{15}N]-RhoA-GDP (0.2 mM) with increasing DH-PH^{PRG} concentrations (0.36 nM to 25 nM). A ^{1}H-^{15}N HSQC spectrum (two scans, 5 min) of [^{15}N]-RhoA-GDP was recorded before adding DH-PH^{PRG} and 1 mM GTPγS. Spectra collected successively at 5-min intervals exhibit decreasing intensities of RhoA-GDP peaks and appearance of RhoA-GTPγS peaks (Fig. 1*C*) until only the latter are visible. The fraction of RhoA in the GDP-bound state ($I_{GDP}/(I_{GDP}+I_{GTP\gamma S})$) was calculated from peak heights in each spectrum and fitted to an exponential decay curve to extract an exchange rate constant for each DH-PH^{PRG} concentration. We found a rate of 5.5×10^{-4} min^{-1} for the intrinsic nucleotide exchange and observed 3.5–214-fold stimulation of exchange for these GEF concentrations, which represent ratios from 1:500,000 to 1:8,000 relative to RhoA (Fig. 1*D*). Akin to RhoA-p190DHPH (18), the rates follow a hyperbolic dependence on GEF concentration, indicative of a two-step model that includes the formation of a low affinity ternary complex of GEF and nucleotide-bound GTPase prior to the formation of the high affinity complex of GEF and nucleotide-free GTPase (Fig. 1*A*) (19). In previous fluorescence-based studies, the PDZ-RhoGEF DH-PH domain (8) was shown to stimulate exchange 124-fold at a 1:10 ratio relative to RhoA, which is 4–11 times faster than Tiam (20), Dbs (20), and LARG (21). Here, we obtained a greater enhancement (214-fold) in nucleotide exchange with a substantially lower ratio of GEF to RhoA (1:8,000). This may be due in part to the inhibitory effect of mant-labeled nucleotides on GEF activity (30) as well as the high protein concentrations used for the NMR assay.

Does DH-PH^{PRG} Stimulate the Nucleotide Exchange of Active and Inactive Forms of RhoA Equally?—It has been assumed that GEFs promote nucleotide exchange with GDP and GTP equally and that the activation of small GTPases is determined by the higher cellular concentration of GTP (2). However, it has been shown that some GEFs, *e.g.* CDC25 (22) and ITSN1L (19), further favor GTPase activation by more efficiently catalyzing the exchange of GDP to GTP. Here, we examined the activity of DH-PH^{PRG} in the reverse reaction with the replacement of GTPγS bound to RhoA with GDP.

Although DH-PH^{PRG} (25 nM) accelerates the nucleotide exchange reaction from RhoA-GDP to RhoA-GTPγS by a factor of 214 in the presence of a 5-fold molar excess of GTPγS, the reverse reaction from RhoA-GTPγS to RhoA-GDP is only stimulated by a factor of 31 ($k_{ex} = 178 \times 10^{-4}$ min^{-1}, intrinsic rate $k_{ex} = 5.8 \times 10^{-4}$ min^{-1}) in the presence of DH-PH^{PRG} and a 50-fold molar excess of GDP (Fig. 3). Despite the large excess of GDP, the reaction reaches a plateau at $I_{GTP\gamma S} \sim 0.25$ due to the

Downloaded from www.jbc.org at TORONTO WESTERN HOSPITAL, on February 16, 2010

Supplemental Material can be found at:
http://www.jbc.org/content/suppl/2009/12/17/M109.064691.DC1.html

very efficient PDZ-RhoGEF favoring the exchange reaction toward the RhoA activated form and as well as the higher affinity of RhoA for GTPγS (Fig. 3). The inefficient exchange from GTPγS to GDP in the absence of GEF indicates a higher RhoA affinity for GTPγS. The discrepancy in the -fold stimulation for the forward and reverse reactions suggests that the affinity of DH-PH^{PRG} for RhoA is affected by nucleotide-dependent structural changes in RhoA. These results indicate that the GEF activity of DH-PH^{PRG} depends on the nature of the bound nucleotide. Our results show that like CDC25 (22) and ITSN1L (19), PDZ-RhoGEF acts as a positive regulator by efficiently catalyzing nucleotide exchange in the forward direction (GDP to GTP), therefore driving the equilibrium toward the activation of the GTPase RhoA.

DH-PH^{PRG} Mutations in the CR1 and CR3 Regions of the DH Domain Dramatically Reduce GEF Activity—Using our NMR GEF assay combined with site-directed mutagenesis, we carried out a structure-function analysis of PDZ-RhoGEF. Based on the crystal structure (7), DH-PH^{PRG} Arg-868 is hydrogen-bonded to RhoA Asp-45 and Glu-54, important residues for recognition. We first tested the effect of the mutation R868G in DH-PH^{PRG}, which resulted in a dramatic reduction in GEF activity. At a DH-PH^{PRG} (R868G) concentration of 1.8 nM (Fig. 4*A*, *green curve*), no GEF activity was detected, whereas a 19-fold increase was observed with the wild type (Fig. 4*A*, *black curve*). This is consistent with the crystal structure of PDZ-RhoGEF in complex with RhoA, in which the side chain of Arg-868 forms hydrogen bonds with Asp-45 and Glu-54 of RhoA (Fig. 4*B*) and was required for GEF activity (7, 8).

In the crystal structure (7), PDZ-RhoGEF Glu-741 directly interacts with Tyr-34, Thr-37, and Val-38 of RhoA switch I, as do the homologous residues of Tiam1 and Rac1 (6, 23). We examined the role of Glu-741 in PDZ-RhoGEF activity by mutating this residue to Ala and Asp. Not surprisingly, E741A virtually eliminated GEF activity ($k_{ex} = 5.7 \times 10^{-4}$ min^{-1}) when compared with the wild type ($k_{ex} = 118 \times 10^{-4}$ min^{-1}). The loss of activity associated with this mutant clearly demonstrates the importance of this carboxyl group for the catalytic activity of PDZ-RhoGEF. We then addressed how a conservative glutamate to aspartate mutation at this position (E741D) would affect the activity. To our surprise, this substitution, which retains the carboxyl group but reduces the length of the side chain by one CH_2, was also sufficient to nearly abolish the enzymatic activity of PDZ-RhoGEF ($k_{ex} = 6 \times 10^{-4}$ min^{-1}). These results suggest that the shorter aspartate side chain cannot preserve the hydrogen bonds formed between Glu-741 and RhoA switch I residues (Fig. 4*B*). We believe that the interactions between the CR1 helix α1a in PDZ-RhoGEF and the RhoA switch I loop are crucial for the catalysis.

RhoA Glu-97 Is Important for Efficient DH-PH^{PRG}-catalyzed Nucleotide Exchange—The PH domain is critical for the function of Dbl family proteins (24–27) and has been suggested to serve multiple roles. The Trio PH domain promotes proper cellular membrane localization through interactions with phospholipids (24), whereas the Vav PH domain regulates the GEF activity of the DH domain through binding of phosphatidylinositides (25), and the Dbs PH domain assists the DH-associated domain in binding Rho GTPases (26, 27). Based on the crystal structure of GEF-

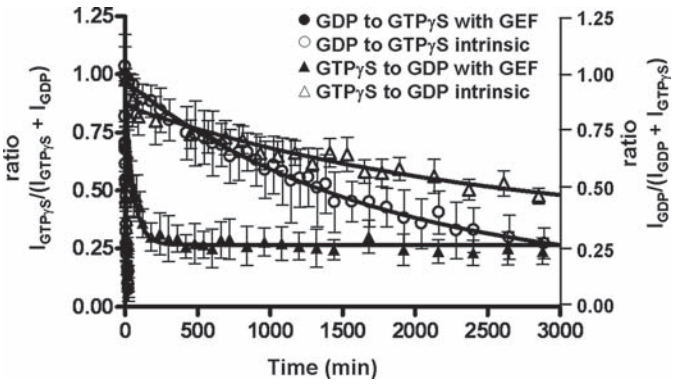

FIGURE 3. **PDZ-RhoGEF preferentially catalyzes nucleotide exchange in the direction of activation (GDP to GTPγS).** Plots of the nucleotide exchange for RhoA-GDP to GTPγS (*circles*) and RhoA-GTPγS to GDP (*triangles*) (intrinsic, *open*; GEF-mediated, *filled*) are shown. A 5-fold molar excess of GTPγS was added to ^{15}N-labeled RhoA-GDP, and a 50-fold molar excess of GDP was added to ^{15}N-labeled RhoA-GTPγS. *Error bars* indicate S.D. for values reported by multiple peaks.

GTPase complexes, the PH domains of some GEFs interact with the GTPase (*e.g.* PDZ-RhoGEF-RhoA (1XCG), LARG-RhoA (1X86), and Dbs-RhoA (1LB1)), whereas no interaction is seen between other GEF PH domains and their cognate GTPases (*e.g.* Vav-Rac1 (2VRW) and Tiam1-Rac1 (1FOE)). Although the PH domains of LARG and PDZ-RhoGEF interact with RhoA, the PDZ-RhoGEF DH domain alone is 41-fold less active than DH-PH domain (7), whereas the equivalent truncation of the PH domain in LARG causes only a 1.5-fold reduction in activity (21). Because it has been reported that the DH domain alone of PDZ-RhoGEF is unstable (7, 8), it is not clear whether the PH domain contributes directly to the activity. The crystal structure of PDZ-RhoGEF bound to nucleotide-free RhoA shows that RhoA Glu-97 interacts with a conserved serine (Ser-1065) as well as an asparagine of the PH domain (Fig. 4*C*). To evaluate the role of this RhoA PH domain interaction, we mutated RhoA Glu-97 to alanine and monitored the nucleotide exchange with and without DH-PH^{PRG}, using our NMR assay. Although the intrinsic nucleotide exchange rates remain identical for both RhoA-WT ($k_{ex} = 5.5 \times 10^{-4}$ min^{-1}) and RhoA-E97A ($k_{ex} = 5.3 \times 10^{-4}$ min^{-1}), a 10-fold decrease in the RhoA activation by DH-PH^{PRG} was observed with RhoA-E97A (RhoA-WT: $k_{ex} = 267 \times 10^{-4}$ min^{-1}, RhoA-E97A: $k_{ex} = 25.5 \times 10^{-4}$ min^{-1}) (Fig. 4*C*). Although this protein-docking site was also found in the PDZ-RhoGEF homologue LARG, with the conserved serine Ser-1118 (Fig. 2) hydrogen-bonded to Glu-97 of RhoA (21), the Glu-97 mutation did not affect the ability of LARG to activate RhoA (21). These results together indicate that PDZ-RhoGEF PH domain contributes to RhoA activation by a mechanism involving the H-bonds between Glu-97 and Ser-1065 and Asn-1068, presumably as seen in the crystal structure of PDZ-RhoGEF-RhoA (7).

Effects of GTP Analogues on the Structure and Exchange Kinetics of RhoA—Many previous studies of GEFs have relied on assays using fluorescent nucleotide analogues (*e.g.* mant-GTP) (7, 8, 20, 21, 23, 27, 28). Our NMR approach has a substantial advantage over this method as it does not require a chemical modification of the nucleotide. We recently demonstrated that mant-GTP and mant-GDP alter the kinetics of the PDZ-RhoGEF-catalyzed nucleotide exchange as well as the in-

Downloaded from www.jbc.org at TORONTO WESTERN HOSPITAL, on February 16, 2010

Supplemental Material can be found at:
http://www.jbc.org/content/suppl/2009/12/17/M109.064691.DC1.html

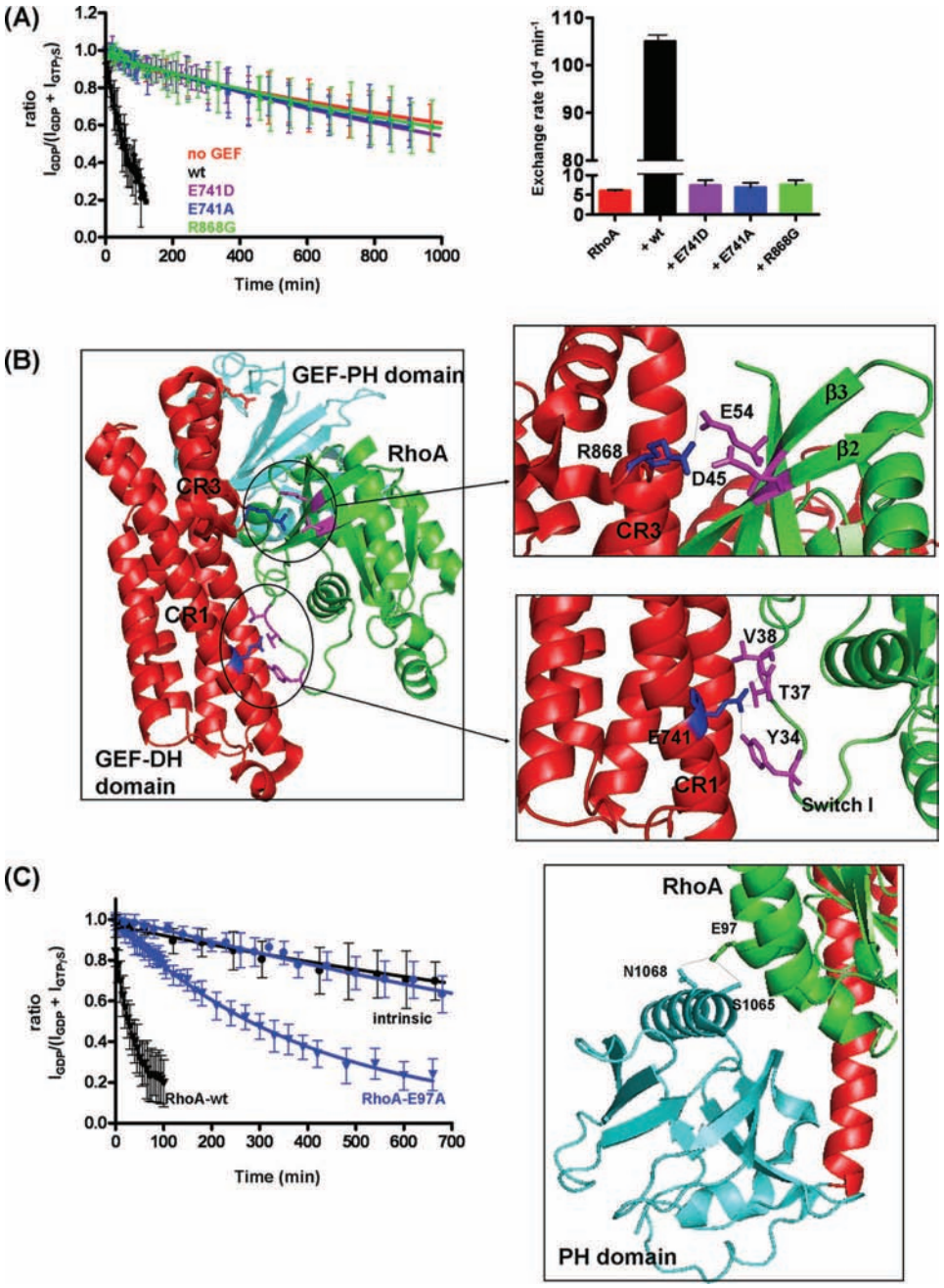

FIGURE 4. **Mutations in conserved regions of DH-PH^{PRG} severely decrease GEF activity, and E97A mutation decreases the activation of RhoA.** *A*, RhoA nucleotide exchange (GDP to GTPγS) stimulated by wild-type (*wt*) DH-PH^{PRG} (1.8 nM) *versus* mutants E741D, E741A, and R868G. Rates derived from these curves are displayed in a histogram in the *right panel*. The experiments were also performed with 4 nM DH-PH^{PRG}, in which wild-type, E741D, E741A, R868G, and intrinsic nucleotide exchange rates are $207 \times 10^{-4} \pm 3.3 \times 10^{-5}$ min^{-1}, $6.4 \times 10^{-4} \pm 1 \times 10^{-4}$ min^{-1}, $14.4 \times 10^{-4} \pm 1 \times 10^{-4}$ min^{-1}, $11.1 \times 10^{-4} \pm 1 \times 10^{-4}$ min^{-1} and $4.4 \times 10^{-4} \pm 2 \times 10^{-4}$ min^{-1}, respectively. *B*, interface of PDZ-RhoGEF DH (*red*) and PH domains (*cyan*) with RhoA (*green*). DH-PH^{PRG} Glu-741 (in CR1), Arg-868 (near CR3), and RhoA switch I residues Tyr-34, Thr-37, and Val-38 are highlighted (PDB code: 1XCG). PyMOL software was used to create the schematic representations. *C*, mutation of Glu-97 reduces the ability of DH-PH^{PRG} to activate RhoA. RhoA nucleotide exchange to GTPγS in the absence (*circles*) or presence (*triangles*) of DH-PH^{PRG} (4 nM). *Black* and *blue curves* correspond to wild-type RhoA and RhoA-E97A, respectively. *Right panel*, RhoA Glu-97 forms hydrogen bonds with Ser-1065 and Asn-1068 of the PH domain. In *A* and *C*, *error bars* indicate S.D. for values reported by multiple peaks.

trinsic GTPase activity of RhoA (30). To further assess the effects of nucleotide modifications, we compared DH-PH^{PRG}-mediated exchange kinetics of GTPγS, GMPPNP, and mant-GTP. The RhoA-GDP nucleotide exchange rates for mant-GTP (203×10^{-4}min^{-1}, corrected for hydrolysis, see supplemental material) and GMPPNP (114×10^{-4} min^{-1}) are 30 and 55% slower than GTPγS (265.5×10^{-4} min^{-1}), respectively (Fig. 5*A*). We then sought to identify aspects of RhoA structure that may account for these different exchange rates. Spectra of RhoA bound to GTPγS, GMPPNP, or mant-GTP were compared with those of RhoA-GDP and RhoA-GTP. The chemical shifts for RhoA residues located in the P-loop, switch I, switch II, β_2, and β_3 in the presence of GMPPNP and mant-GTP are more similar to those with GDP than GTP, whereas the fingerprint of RhoA-GTPγS is more like that of RhoA-GTP, as illustrated by Gln-29 of RhoA in Fig. 5*B*. These results further support that among these analogues, GTPγS provides the best mimic of GTP and that the conformation of RhoA-GTPγS most resembles the activated conformation of RhoA-GTP (Fig. 5*C*).

To more rigorously compare the individual nucleotide exchange rates using GTP and the three commonly used analogues, GTPγS, GMPPNP, and mant-GTP, we performed a real-time NMR-based competition assay. Importantly, NMR spectroscopy can distinguish RhoA bound to each of the four nucleotide variants. We added 6 nM DH-PH^{PRG} to RhoA-GDP and initiated the exchange assay with the addition of a mixture containing GTP, GTPγS, GMPPNP, and mant-GTP (each 1 mM) (Fig. 5*D*). GTP and GTPγS peaks appeared first in the ^{1}H-^{15}N HSQC spectra, indicating their preferential recruitment by RhoA. After 1 h (Fig. 5*D*), a stronger GTPγS peak was observed along with weaker GTP and mant-GTP peaks, but no peak was detected for GMPPNP. It should be noted that GTP and mant-GTP peak intensities eventually decreased due to intrinsic GTPase activity of RhoA (supplemental Fig. S6). The nucleotide exchange and competition assays show that association of mant-GTP with RhoA is slower than that of GTP and GTPγS. Based on the structure of Ras in complex with mant-GTP (29), we hypothesize that similar positioning of the mant group to RhoA may interfere with the fast rotation of its Tyr-34 side

Downloaded from www.jbc.org at TORONTO WESTERN HOSPITAL, on February 16, 2010

Supplemental Material can be found at:
http://www.jbc.org/content/suppl/2009/12/17/M109.064691.DC1.html

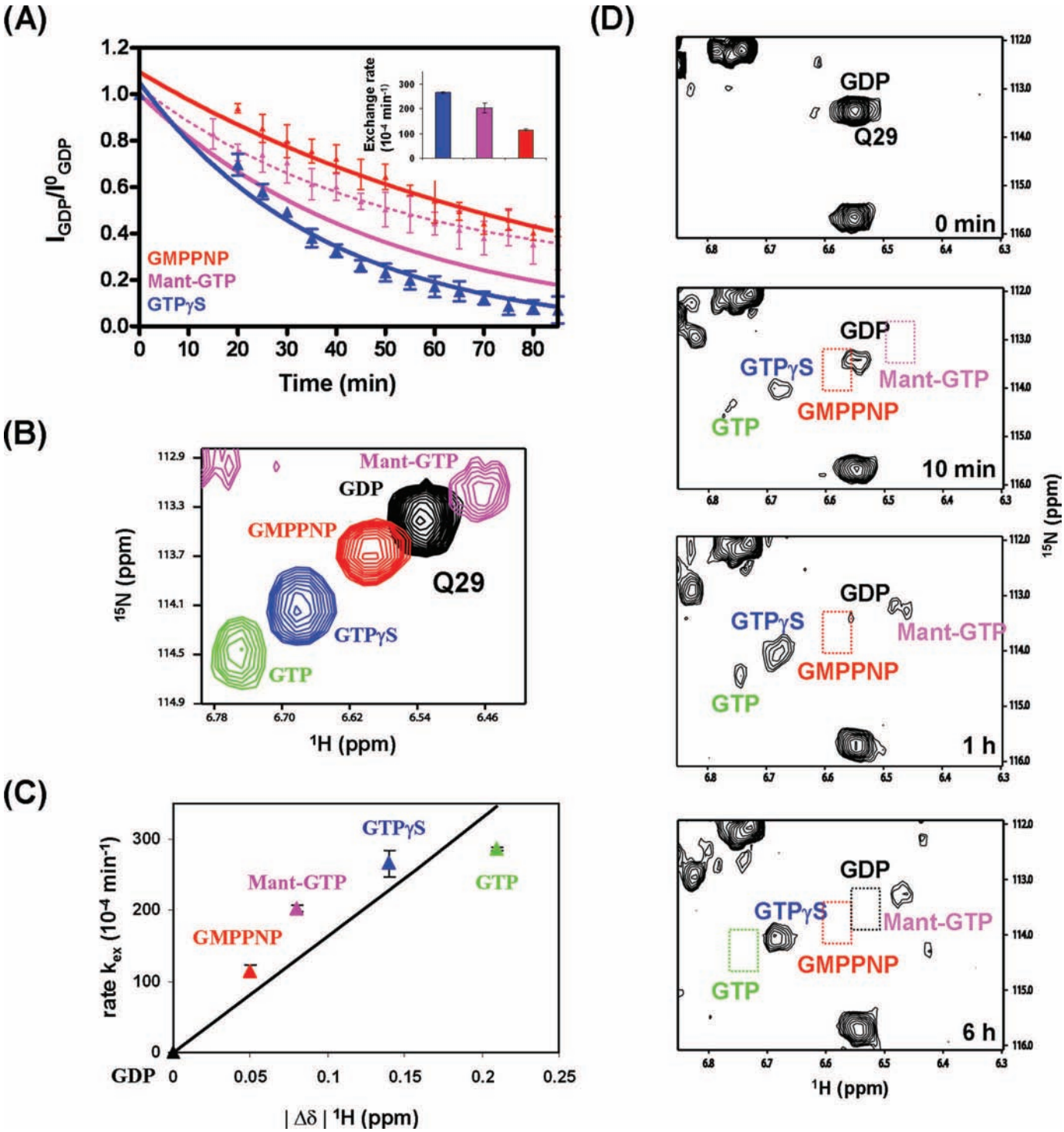

FIGURE 5. **Kinetics of RhoA nucleotide exchange with GTP analogues and competition assay.** *A*, kinetics of RhoA-GDP nucleotide exchange to GTPγS (*blue*), GMPPNP (*red*), and mant-GTP (*magenta*) measured individually using our NMR-based assay. The rates (10^{-4} min^{-1}) are displayed with a histogram (*inset*) for each curve. *B*, overlay of five ^{1}H-^{15}N HSQC spectra illustrating the distinct chemical shifts of Gln-29 exhibited by RhoA when bound to GDP (*black*), GMPPNP (*red*), GTPγS (*green*), GTPγS (*blue*), and mant-GTP (*magenta*). *C*, Gln-29 amide proton chemical shift changes ($\Delta\delta^1$H, relative to RhoA-GDP) *versus* exchange rates for each nucleotide (colored as above).In *A* and *C*, *error bars* indicate S.D. *D*, competition assay for binding of nucleotide analogues to RhoA. Snapshots of ^{1}H-^{15}N HSQC spectra collected before and after the addition of premixed GTP, GTPγS, GMPPNP, and mant-GTP, each at a 5-fold molar excess over RhoA.

chain from the position where it binds Glu-741 to the orientation that contacts the nucleotide (supplemental Fig. S7).

Our data firmly demonstrate the differences in the binding affinity of RhoA for GTP and its three commonly used analogues. Although the exact binding constants for each analogue cannot be derived from the present NMR data, NMR can distinguish small differences in the binding affinity between these ligands as translated in the exchange rates: $k_{ex}^{GTP} \cong k_{ex}^{GTP\gamma S} > k_{ex}^{mant\text{-}GTP} > k_{ex}^{GMPPNP}$. It is worth noting that these thermodynamic differences in binding correlate well with con-

Downloaded from www.jbc.org at TORONTO WESTERN HOSPITAL, on February 16, 2010

Supplemental Material can be found at:
http://www.jbc.org/content/suppl/2009/12/17/M109.064691.DC1.html

formational changes in RhoA observed in NMR spectra (Fig. 5, *B* and *C*).

In summary, we have demonstrated that NMR spectroscopy offers an accurate and efficient measurement of GEF-mediated nucleotide exchange of a small GTPase. This methodology was applied to RhoA intrinsic and PDZ-RhoGEF-catalyzed nucleotide exchange reactions. We have shown that GTPγS mimics GTP in the RhoA exchange reaction, whereas GMPPNP and mant-GTP suffer from slower exchange rates. The intrinsic nucleotide exchange rate from GDP to GTPγS is dramatically accelerated (214-fold) by the presence of a small amount of DH-PH^{PRG} (25 nM). This effective catalysis is achieved by highly specific interactions between RhoA and PDZ-RhoGEF DH and PH domains. Our results show that Arg-868 near CR3 and Glu-741 in CR1 play critical roles in the catalysis and that Glu-97 of RhoA is required for full GEF activity. Furthermore, PDZ-RhoGEF acts as a positive regulator that selectively catalyzes nucleotide exchange toward the activation of the GTPase RhoA. The present NMR studies provided kinetic and mechanistic insights into the enzymatic reaction of the PDZ-RhoGEF-mediated nucleotide exchange of RhoA and also posed new questions about the structural basis for the catalysis, which can be addressed by an atomic resolution structure elucidation of the binary complex.

Acknowledgment—A grant from the Canada Foundation for Innovation funded the Bruker 800- and 600-MHz NMR spectrometers.

REFERENCES

1. Etienne-Manneville, S., and Hall, A. (2002) *Nature* **420,** 629–635
2. Bos, J. L., Rehmann, H., and Wittinghofer, A. (2007) *Cell* **129,** 865–877
3. Fu, M., Sabra, M. M., Damcott, C., Pollin, T. I., Ma, L., Ott, S., Shelton, J. C., Shi, X., Reinhart, L., O'Connell, J., Mitchell, B. D., Baier, L. J., and Shuldiner, A. R. (2007) *Diabetes* **56,** 1363–1368
4. Gu, J., Wu, X., Dong, Q., Romeo, M. J., Lin, X., Gutkind, J. S., and Berman, D. M. (2006) *Cancer* **106,** 2716–2724
5. Schmidt, A., and Hall, A. (2002) *Genes Dev.* **16,** 1587–1609
6. Hoffman, G. R., and Cerione, R. A. (2002) *FEBS Lett.* **513,** 85–91
7. Derewenda, U., Oleksy, A., Stevenson, A. S., Korczynska, J., Dauter, Z., Somlyo, A. P., Otlewski, J., Somlyo, A. V., and Derewenda, Z. S. (2004) *Structure* **12,** 1955–1965
8. Oleksy, A., Opaliński, Ł., Derewenda, U., Derewenda, Z. S., and Otlewski, J. (2006) *J. Biol. Chem.* **281,** 32891–32897
9. Liu, X., Wang, H., Eberstadt, M., Schnuchel, A., Olejniczak, E. T., Meadows, R. P., Schkeryantz, J. M., Janowick, D. A., Harlan, J. E., Harris, E. A., Staunton, D. E., and Fesik, S. W. (1998) *Cell* **95,** 269–277
10. Marshall, C. B., Ho, J., Buerger, C., Plevin, M. J., Li, G. Y., Li, Z., Ikura, M., and Stambolic, V. (2009) *Sci. Signal.* **2,** ra3
11. Delaglio, F., Grzesiek, S., Vuister, G. W., Zhu, G., Pfeifer, J., and Bax, A. (1995) *J. Biomol. NMR* **6,** 277–293
12. Johnson, B. A., and Blevins, R. A. (1994) *J. Biomol. NMR* **4,** 603–614
13. Ikura, M., Kay, L. E., and Bax, A. (1990) *Biochemistry* **29,** 4659–4667
14. Clore, G. M., and Gronenborn, A. M. (1998) *Curr. Opin. Chem. Biol.* **2,** 564–570
15. Wishart, D. S., Sykes, B. D., and Richards, F. M. (1992) *Biochemistry* **31,** 1647–1651
16. Wei, Y., Zhang, Y., Derewenda, U., Liu, X., Minor, W., Nakamoto, R. K., Somlyo, A. V., Somlyo, A. P., and Derewenda, Z. S. (1997) *Nat. Struct. Biol.* **4,** 699–703
17. Ito, Y., Yamasaki, K., Iwahara, J., Terada, T., Kamiya, A., Shirouzu, M., Muto, Y., Kawai, G., Yokoyama, S., Laue, E. D., Wälchli, M., Shibata, T., Nishimura, S., and Miyazawa, T. (1997) *Biochemistry* **36,** 9109–9119
18. Hemsath, L., and Ahmadian, M. R. (2005) *Methods* **37,** 173–182
19. Kintscher, C., and Groemping, Y. (2009) *J. Mol. Biol.* **387,** 270–283
20. Snyder, J. T., Worthylake, D. K., Rossman, K. L., Betts, L., Pruitt, W. M., Siderovski, D. P., Der, C. J., and Sondek, J. (2002) *Nat. Struct. Biol.* **9,** 468–475
21. Kristelly, R., Gao, G., and Tesmer, J. J. (2004) *J. Biol. Chem.* **279,** 47352–47362
22. Lai, C. C., Boguski, M., Broek, D., and Powers, S. (1993) *Mol. Cell Biol.* **13,** 1345–1352
23. Worthylake, D. K., Rossman, K. L., and Sondek, J. (2000) *Nature* **408,** 682–688
24. Skowronek, K. R., Guo, F., Zheng, Y., and Nassar, N. (2004) *J. Biol. Chem.* **279,** 37895–37907
25. Han, J., Luby-Phelps, K., Das, B., Shu, X., Xia, Y., Mosteller, R. D., Krishna, U. M., Falck, J. R., White, M. A., and Broek, D. (1998) *Science* **279,** 558–560
26. Rossman, K. L., Cheng, L., Mahon, G. M., Rojas, R. J., Snyder, J. T., Whitehead, I. P., and Sondek, J. (2003) *J. Biol. Chem.* **278,** 18393–18400
27. Rossman, K. L., Worthylake, D. K., Snyder, J. T., Siderovski, D. P., Campbell, S. L., and Sondek, J. (2002) *EMBO J.* **21,** 1315–1326
28. Oleksy, A., Barton, H., Devedjiev, Y., Purdy, M., Derewenda, U., Otlewski, J., and Derewenda, Z. S. (2004) *Acta Crystallogr. D Biol. Crystallogr.* **60,** 740–742
29. Scheidig, A. J., Franken, S. M., Corrie, J. E., Reid, G. P., Wittinghofer, A., Pai, E. F., and Goody, R. S. (1995) *J. Mol. Biol.* **253,** 132–150
30. Mazhab-Jafari, M. T., Marshall, C. B., Smith, M., Gasmi-Seabrook, G. M., Stambolic, V., Rottapel, R., Neel, B. G., and Ikura, M. (2009) *J. Biol. Chem.* **285,** 5132–5136

Downloaded from www.jbc.org at TORONTO WESTERN HOSPITAL, on February 16, 2010